Ore Geology Reviews 159 (2023) 105544

Contents lists available at ScienceDirect

Ore Geology Reviews

journal homepage: www.elsevier.com/locate/oregeorev

The genetic association between vein and skarn type tungsten mineralization in the Yaogangxian tungsten deposit, South China: Constraints from LA-ICP-MS analysis of individual fluid inclusion

Wen-Sheng Li [a,b], Pei Ni [a,*], Jun-Yi Pan [a,*], Stefano Albanese [c], Benedetto De Vivo [a,c], Rosario Esposito [d], Jun-Ying Ding [a]

[a] State Key Laboratory for Mineral Deposits Research, Institute of Geo-Fluids, Frontiers Science Center for Critical Earth Material Cycling, School of Earth Sciences and Engineering, Nanjing University, 210023, China
[b] School of Geographic and Oceanographic Sciences, Nanjing University, Nanjing 210023, China
[c] University of Naples Federico II, Italy
[d] Università di Milano Bicocca, Italy

ARTICLE INFO

Keywords:
Scheelite
Wolframite
Fluid inclusion
LA-ICP-MS
Yaogangxian
Nanling Range

ABSTRACT

The large-scale Yaogangxian W deposit, located in central of the Nanling metallogenic belt, South China, comprises independent quartz vein-type and skarn-type W mineralization. Wolframite-bearing quartz veins occur invariably in metasandstone and slate to the northwest of the Yaogangxian granitic intrusion, whereas scheelite-skarn are mainly hosted by the limestone to the east. The vertical extension of single wolframite-bearing quartz vein can reach up to 1000 m and we focused on the vein samples collected from the deepest level (26 level) which likely recorded early magmatic fluids. For skarn mineralization, two scheelite precipitation stages were recognized, namely scheelite-1 in retrograde stage and scheelite-2 from sulfide-stage. To reveal the fluid sources and characteristics of two mineralizing systems, detailed petrography and microthermometry analyses were carried out on fluid inclusion assemblages (FIA) in scheelite, wolframite and their coexisting quartz. Fluid compositions were obtained from individual fluid inclusion (FI) in ore and gangue minerals via laser ablation inductively coupled plasma mass spectrometry (LA-ICP-MS) analysis. These data aid elucidation on the source and nature of fluids in the two distinct W mineralization styles. The chemical compositions of FIs hosted in wolframite and scheelite points to a common magmatic source. The fluid in the scheelite ore section exhibits lower As and B than the wolframite ore section, indicating that boiling may have occurred at early skarn stage. Fluid evolution in the two mineralizing systems suggest that formation of diverse W mineralization styles is mainly controlled by different host lithology and fluid processes. In the wolframite ore section, ore-forming fluid recorded in the deepest level of vein show elevated As, B, K and Rb contents than previously reported ore-forming fluid obtained from the tip of the vein. This likely indicate absence of intensive fluid immiscibility in the deep during wolframite formation, which may rather be accompanied by fluid-rock interaction. In the scheelite ore section, constant injection of meteoric water is revealed. FI hosted in scheelite-1 and 2 exhibit similar compositions, and the lower K content in scheelite-2 fluid is thought to be caused by sericitization in the retrograde stage skarn. The Mo content of scheelite decreased from the retrograde stage to sulfide-stage, indicating a decrease in oxygen fugacity. Based on these conclusion and previous geological and geochronological studies, we propose a metallogenic model of the coupled wolframite-quartz vein and scheelite-skarn mineralization.

1. Introduction

Tungsten was classified as one of the strategic critical elements for its widely usage in numerous highly technical fields (Hayes and McCullough, 2018). While tungsten mineralization is worldwide spatially associated with highly fractionated felsic granitic intrusions and form

* Corresponding authors.
E-mail addresses: peini@nju.edu.cn (P. Ni), pjynju2010@126.com (J.-Y. Pan).

https://doi.org/10.1016/j.oregeorev.2023.105544
Received 22 March 2023; Received in revised form 27 May 2023; Accepted 15 June 2023
Available online 20 June 2023

numerous types of ore deposit (Hulsbosch et al., 2016; Zhao et al., 2017; Launay et al., 2021; Ni et al., 2023), the global tungsten supply is predominantly mined from scheelite-skarn and wolframite-quartz vein type ore deposits (Fonteilles et al., 1989; Meinert et al., 2005; Mao et al., 2019; Chang et al., 2019). Notably, scheelite- and wolframite-dominated W mineralization can sometimes occur within single deposit sharing similarities of age and geological setting, but form separate orebodies (Ni et al., 2023; Li et al., 2020, Li et al., 2021, 2022a). Prominent examples include the combined W mineralization of scheelite-skarn and wolframite-quartz vein at Yaogangxian, Yaoling and Kuimeishan deposits (Li et al., 2020; Li et al., 2022b), and the combination of scheelite- and wolframite-quartz veins in Chuankou deposits (Li et al., 2022a) of South China. The comparative study of the metallogenic processes of these distinct W mineralization styles in single deposit is crucial for the establishment and improvement of metallogenic models, and may provide new perspectives for exploration of economically significant W deposits (Xu, 1957; Li et al., 2021; Ni et al., 2023).

The Yaogangxian W deposit is located in the central Nanling Range which covers the middle part of the South China Block (Fig. 1A). It comprises independent W mineralization of both wolframite-quartz vein and scheelite-skarn types. The former is spatially and temporally related to a composite granitic intrusion emplaced into a sedimentary sequence dominated by Cambrian and Devonian sandstone. In contrast, skarn W mineralization was hosted in the interface between the Devonian limestone and quartzite, and has no direct contact with the intrusion. Spatially, the scheelite-skarn is located within 2 km east of wolframite-quartz veins. These two distinct styles of mineralization in Yaogangxian W deposit provides an ideal case to test their genetic link and to compare their mineralization processes.

Previously, the metallogenesis studies at Yaogangxian were mainly focused on vein type mineralization (Peng et al., 2006; Wang and Ren, 2018; Li et al., 2018; Pan et al., 2019; Xiao et al., 2021; Jiang et al., 2022), whereas the metallogenic process of the skarn type W mineralization was barely investigated (Yu et al., 2021). Despite that the spatial and temporal relationships between vein and skarn type W mineralization at Yaogangxian imply a genetic link in between (Xu, 1957; Li et al., 2020), the detailed fluid processes involved in the formation of scheelite-skarn and chemical characteristics of ore-forming fluids forming diverse types of ore bodies remain poorly constrained. These hamper direct understanding on the genetic association and metallogenic mechanisms of the coupled W mineralization systems.

In this contribution, we present detailed geologic and fluid information to constrain the relationship between vein and skarn type W mineralization in the Yaogangxian deposit. Petrography and microthermometry of fluid inclusions hosted in both wolframite and scheelite reveal thermally distinct hydrothermal processes responsible for diverse mineralization style. LA-ICP-MS analysis on individual fluid inclusions were used to obtain the fluid composition of both mineralizing fluids and to access their source and genetic association. This information is further discussed to develop a model for the origin and evolution of the fluid responsible for the Yaogangxian W deposit and define the principal controls on its diverse mineralization styles.

2. Geological setting

The Nanling Range, located in the northwest of the Cathaysia Block in South China, was recognized as one of the largest W metallogenic province in the world (Mao et al., 2007; Yuan et al., 2019a; Yuan et al., 2019b; Ni et al., 2021, Ni et al., 2023). It encompasses central-southern Hunan, northern Guangxi, southern Jiangxi, and northern Guangdong, with a total area of about 200,000 km^2. Multiple tectonic events exerted great influence on the Nanling Range, resulting in the development of

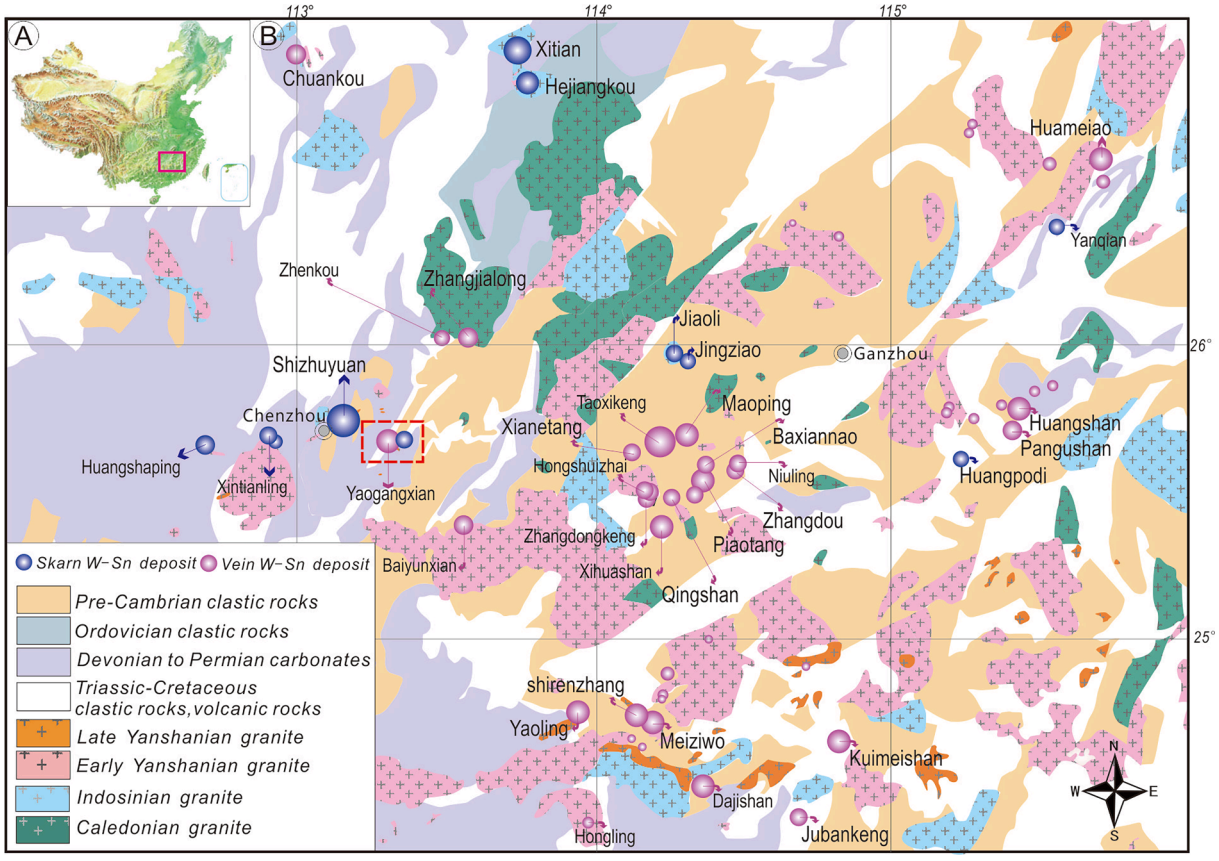

Fig. 1. A-Location of the Nanling region at the country scale. B-Geologic map of the Nanling region including the locations of known skarn and vein type W (-Sn) deposits (modified after Ni et al., 2021).

complicated NNE–SSW-trending fault systems, and leading to intense regional magmatic activity and W mineralization (Shu et al., 2021; Ni et al., 2023). The Neoproterozoic to Silurian metamorphosed rocks formed the basement of the Nanling Range, which was overlain by Devonian to Triassic carbonate rocks with clastic intercalations. Spatially, the strata exposed in the east of the Nanling Range are mainly Precambrian clastic rocks. In the west, it is mainly carbonate and carbonaceous rocks intercalated with terrigenous rocks ranging from Devonian to Permian (Fig. 1). A series of NE-trending basins, controlled by the back-arc extension, generally filled by Jurassic terrigenous clastic sedimentary and volcanic rocks (Shu et al., 2021).

A most important peculiarity of Nanling Range is the intense magmatic activities, resulting in extensive exposure of granitoids and related W (-Sn) mineralization (Fig. 1) (Zhou et al., 2006; Hu and Zhou, 2012; Chen et al., 2013; Liu et al., 2020). The Yanshanian cycle represents the most important magmatic activity, and led to emplacement of voluminous granitic rocks in the Nanling Range. These rocks are dominated by high-K calc-alkaline S-, A- and I-type granites, mainly formed during a short time interval between 165 Ma and 155 Ma (Zhou et al., 2006; Li et al., 2020; Jiang et al., 2018). The genesis of these rocks is attributed to the remelting of continental lithosphere in extensional environment caused by the northwest subduction of the paleo-Pacific plate (Li et al., 2020; Ni et al., 2021). These granites generally occur as composite intrusion, accompanied by economically valuable W mineralization. For example, the Penggongmiao, Miao'ershan-Yuechengling, Yaogangxian and Xihuashan granitic intrusion.

The Nanling Range is the most important W producer in China and hosts several dozen famous W deposits with numerous mineralization styles, e.g., skarn, vein, and disseminated greisen types. Spatially, the eastern part of the Nanling Range is dominated by wolframite-quartz vein type W deposit, while deposits in the west are primarily composed of scheelite-skarn (Fig. 1B). It is likely that the regional zoning of these deposits in types is mainly controlled by the lithology of host sediments, i.e., the Devonian to Permian carbonate rocks are widely developed in the west favoring formation of scheelite-skarn (Lu et al., 2003), whereas low-grade metamorphosed clastic rocks largely exposed in the east and they are conductive to formation of wolframite-quartz vein type W deposits (Ni et al., 2020).

3. Ore deposit geology

The Yaogangxian W deposit comprises both large-scale wolframite-quartz vein type mineralization (>200,000 tonne WO_3) and scheelite-skarn mineralization (310,000 tonne WO_3) (Zhu et al., 2015a). The former was discovered in the early 1900s, and was subsequently mined since 1914. However, the scheelite-skarn discovered in 1947 by Xu Keqin and testified by subsequent drilled between 1954 and 1958 was not exploited until 2020.

The exposed sedimentary rocks in the mining area are mainly Cambrian sandstone, middle Devonian Tiaomajian formation quartzite, middle upper Devonian Shetianqiao formation limestone, and Lower Jurassic quartz sandstone (Fig. 2). Structurally, the Yaogangxian deposit is strictly confined within the NE-trending Yaogangxian anticline including several smaller faults. The granitic intrusion in Yaogangxian, has compositions that range from coarse-grained biotite granite through medium coarse-grained two mica granite to fine-grained muscovite granite with geochemical signatures that are highly differentiated. Zircon dating results from the muscovite granite and two-mica granite show a weighted mean age of 157 ± 1 Ma and 161 ± 3 Ma, respectively (Li et al., 2020), indicating a Jurassic magmatism.

3.1. Wolframite-quartz vein

The wolframite-quartz veins are developed on the rim of the Yaogangxian anticline, and the ore bodies occur in the contact zone between the Cambrian-Devonian sandstone and the granitic intrusion (Fig. 3A). According to field observation, there are more than 300 quartz veins containing wolframite in the Dayanmen section, in which 213 are of high economic significance. The wolframite-quartz vein system is composed of a set of quartz veins of NNW, NW and NWW striking groups (Fig. 2A). The veins in each group show similar mineral assemblage and the width of quartz vein is mostly between 0.15 and 1.2 m. The ore grade is very high with W concentration locally reaches 1.4 wt%. Wolframite is the most important ore mineral, locally associated with variable amounts of scheelite, chalcopyrite, arsenopyrite, molybdenite, cassiterite, sphalerite and other sulfosalts. The vein mineralogy in the Dayanmen section contains mainly quartz and wolframite as coarse-grained crystals in veins and locally abundant arsenopyrite (Fig. 4A-B). Typically, wolframite crystals tend to attach to both vein walls (Fig. 4A),

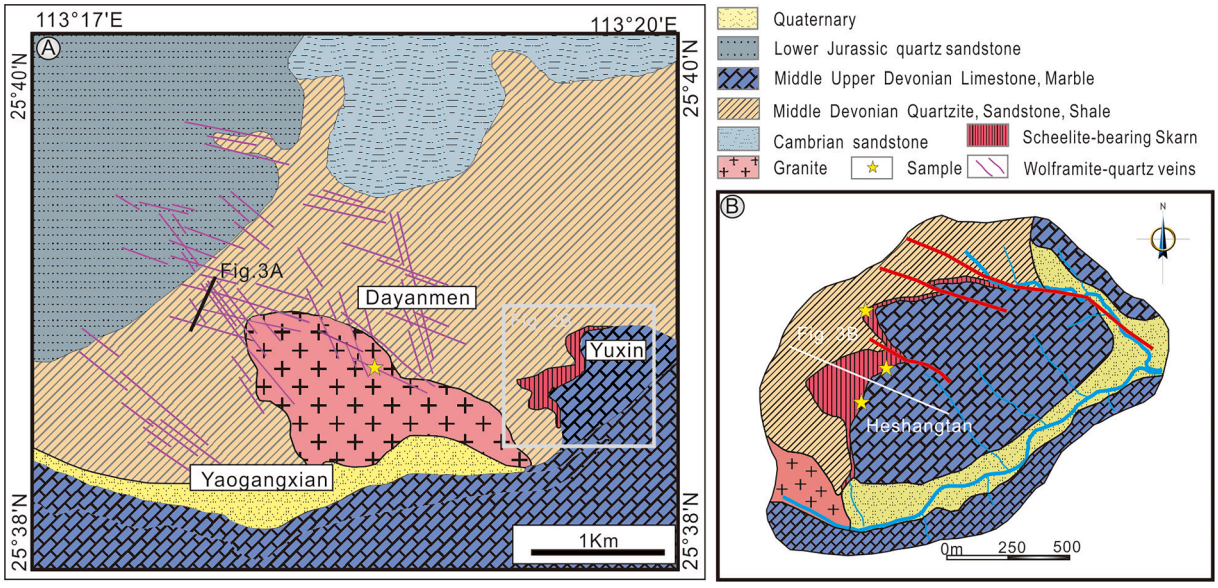

Fig. 2. A-Geologic map of the Yaogangxian deposit (modified after Li et al., 2018) showing the locations of the different mineralized sectors mentioned in text. B-Geologic map of the Yuxin mining area (modified after Xu, 1957) showing locations of the skarn scheelite orebody and representative sample, together with the prospecting line for the Fig. 3B.

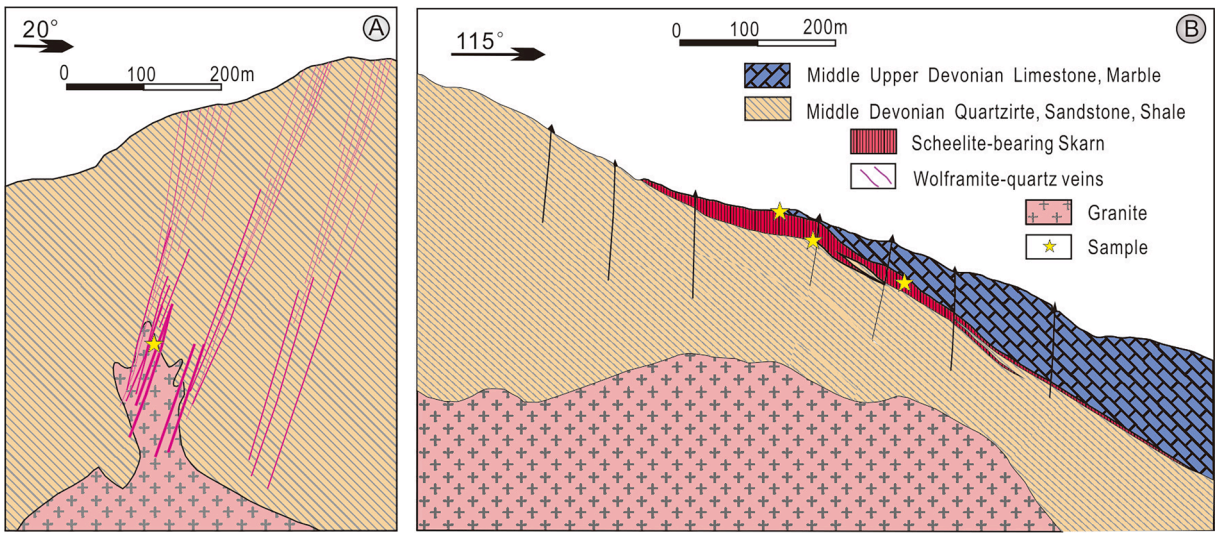

Fig. 3. A-Simplified cross section of the above prospecting line in Fig. 2A, showing relationship between the quartz veins and associated granitic rocks as well as rough locations for wolframite-bearing quartz sample incorporated in this study (modified from Li et al., 2020). B-Cross section showing the skarn-hosted scheelite orebody. Location of section line is shown in Fig. 2B (modified after Xu, 1957).

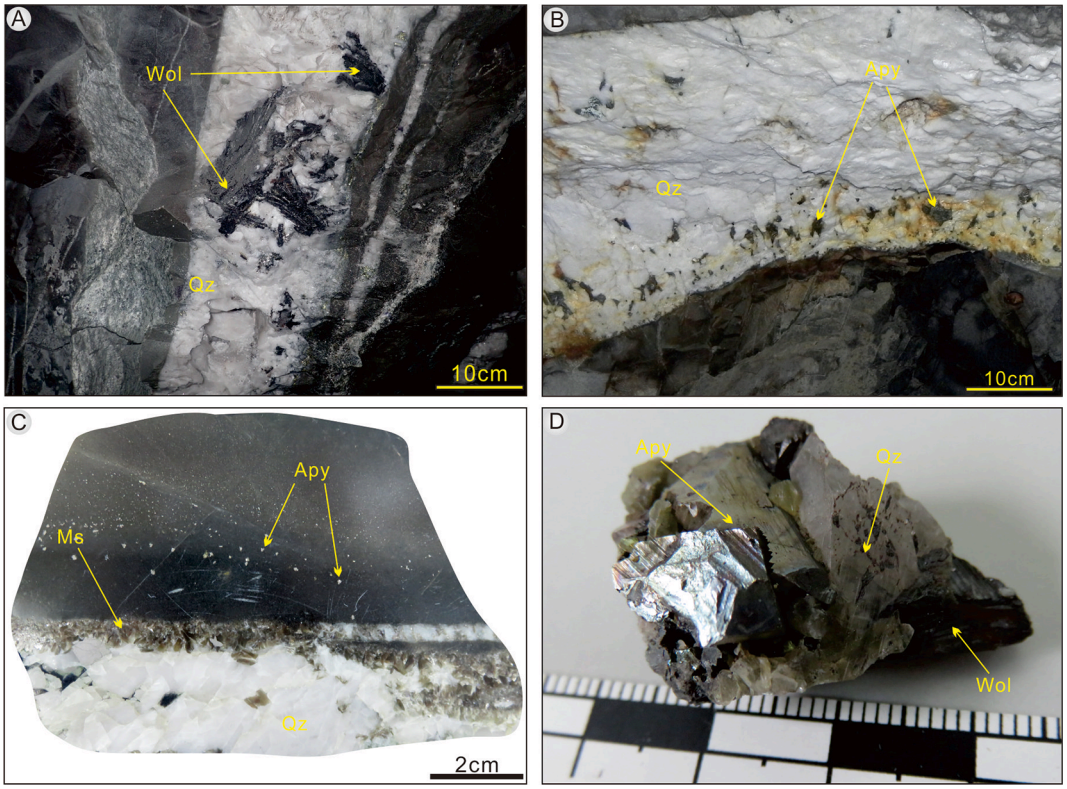

Fig. 4. Representative photographs for the wolframite quartz vein in Yaogangxian deposit. A-Metamorphosed sandstone with several wolframite crystal attached to both vein walls. B-Typical arsenopyrite-rich quartz vein. C-Polished section of sample, showing muscovite selvages in contact zone and small disseminated arsenopyrite phenocrysts in the alteration assemblages. D- Well-crystallized wolframite, arsenopyrite and quartz crystals provide good samples for fluid inclusion study. Abbreviations: Wol = wolframite, Ms = muscovite, Apy = arsenopyrite, Qz = quartz.

indicating relatively early formation in the depositional sequence, despite late stage wolframite also exist in some veins (Pan et al., 2019). Wolframite-bearing quartz veins hosted in metamorphosed sandstone commonly develop muscovite selvages at vein walls (Fig. 4C), but the muscovite frequently coats the wolframite crystals if they both occur. Hydrothermal alteration is developed along the vein walls and commonly formed muscovite, quartz, tourmaline, arsenopyrite and pyrite (Fig. 4 C), accompanied by minor amounts of calcite and topaz. It is notably that abundant arsenopyrites are also disseminated in the alteration assemblages (Fig. 4C), indicating locally intense fluid-rock reaction. Well-crystallized wolframite and quartz crystals are common in vein cavities and provide good samples for fluid inclusion study (Fig. 4D).

3.2. Skarn scheelite

Skarn scheelite orebodies from the Yuxin section mainly develops at the contact zone between the Tiaomajian formation quartzite and the Shetianqiao formation limestone (Fig. 2B). They form structurally controlled pods and lenses that replace marble and limestone (Fig. 3B). The dominant skarn facies in the Yuxin section associated with scheelite mineralization are garnet-wollastonite-idocrase-actinolite skarns (Fig. 5A, B and C). Based on detailed paragenetic study, two skarn stages at the Yuxin section were identified, with the prograde assemblage composed of garnet-wollastonite-idocrase and diopside skarn while the retrograde stage consists of actinolite and epidote skarn (Fig. 5D, E and F). It should be noted that garnet formed in prograde stage generally has been altered to sericite in retrograde stage. Millimeter-size sericite precipitated in core and edge of garnet crystal (Fig. 5G). Late stage sulfide quartz veins characterized by a large amount of quartz and sulfide were also recognized, and these quartz veins frequently cut the skarn stages described above (Fig. 5H and I). Scheelite mineralization in skarn orebodies developed both in skarn and sulfide stages, but the major W resource is contributed by disseminated scheelite that formed in the hydrous retrograde skarn stage (Fig. 5C).

Based on occurrences and petrographic relationships, two types of scheelite were identified, namely scheelite-1 from retrograde skarn stage (Fig. 5B-C) and scheelite-2 in hydrothermal sulfides stage (Fig. 5H-I). Scheelite-1 mainly coexists with garnet which exhibit systematic growth zoning (Fig. 5D, G). Subhedral fluorite is the second most

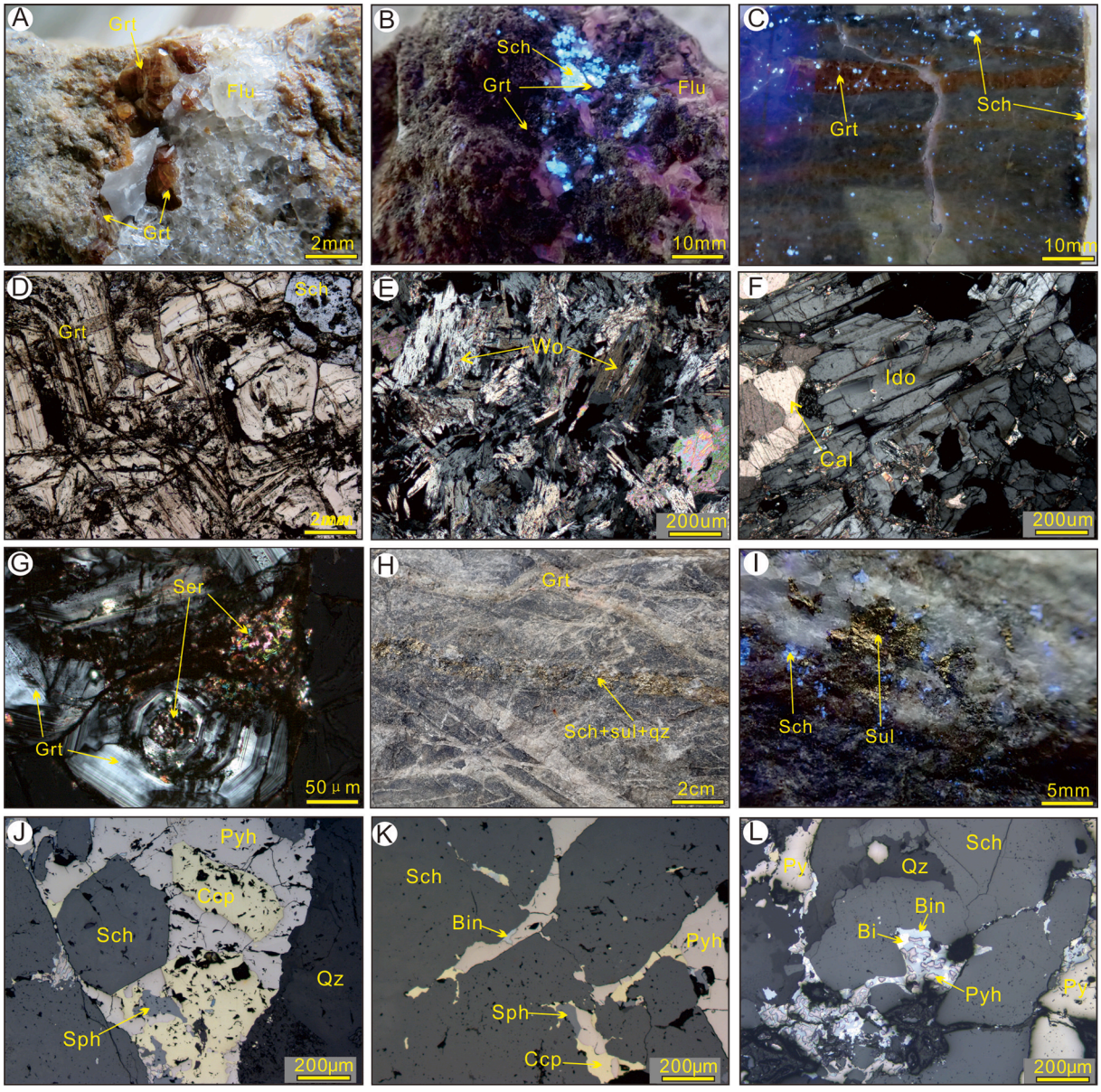

Fig. 5. Photomicrographs showing representative mineral assemblages in the Yuxin section. A- Subhedral fluorite fills the remaining porosity between the garnet and scheelite grain. B- Occurrence of scheelite-bearing skarn under ultraviolet light. C- Garnet-wollastonite-idocrase-actinolite skarn with disseminated scheelite. D- Scheelite filling the interstices between garnet crystals. E, F-Different skarn minerals mainly including wollastonite and idocrase. G- Sericite precipitated in core and edge of garnet crystal. H- Quartz-sulfide-scheelite veins are mainly hosted by the limestone. I-Sulfide quartz vein enriched in scheelite. J-Euhedral scheelite coexists with chalcopyrite, pyrrhotite and sphalerite. K, L- Fractures of scheelite are filled with pyrrhotite, sphalerite, chalcopyrite and bismuthinite. Fluorescent blue minerals under shortwave UV light in these photographs are scheelite. Abbreviations: Grt = garnet, Flu = fluorite, Sch = scheelite, Wo = wollastonite, Ido = idocrase, Cal = calcite, Py = pyrite, Qz = quartz, Sph = sphalerite, Pyh = pyrrhotite, Bin = bismuthinite, Ccp = chalcopyrite. (For interpretation of the references to colour in this figure legend, the reader is referred to the web version of this article.)

abundant mineral and fills the remaining porosity between the garnet and scheelite grain (Fig. 5A). Quartz-sulfide-scheelite veins are commonly a few centimeters wide and were mainly hosted by the limestone (Fig. 5H). Crystals of euhedral scheelite 2 in these veins are ranged in size from 2 to 6 mm, and are generally zoned. The major ore minerals assemblage of the sulfide stage is composed of scheelite, pyrite, chalcopyrite, and pyrrhotite, plus minor bismuthinite and sphalerite (Fig. 5J, K and L) (Fig. 6).

4. Sampling and analytical methods

4.1. Sampling

Locations of the fluid inclusion (FI) samples analyzed in this study are shown in Figs. 2 and 3 (star symbols). The minerals selected for FI studies include coexisting wolframite and quartz collected from the deepest levels of the Dayanmen ore section and scheelite and quartz in the Yuxin ore section. To investigate major and trace element variations of the hydrothermal fluids responsible for different W mineralization styles, over 260 FIs were analyzed via microthermometry and on the base of which a total of 139 FIs were subsequently analyzed by LA-ICP-MS.

5. The Dayanmen section

Primary FIs hosted by wolframite are direct record the ore-forming fluid, and are critical for clarify the physical and chemical conditions of wolframite precipitation. Overall, 8 samples consisting mostly of euhedral quartz and wolframite crystals were collected from the 26 level of the Dayanmen section for fluid inclusion study.

5.1. The Yuxin section

To investigate the ore-forming fluids responsible for scheelite mineralization in the Yuxin ore section, scheelite crystals associated with garnet and quartz-sulfide vein from two mineralizing stages were sampled, respectively. In addition to the scheelite, we sampled quartz associated with scheelite-2 for comparison with quartz in Dayanmen section. In total 15 scheelite-bearing skarn and 12 scheelite-bearing sulfide-quartz vein samples from the Yuxin section were investigated.

5.2. Microthermometry

The microthermometric study was performed on doubly polished thin sections, within −195 to +600 ℃ temperature interval using a Linkam THMSG600 heating-freezing stage mounted on an Olympus BX51 polarizing microscope. The microscope is equipped with an infrared camera to ensure infrared observation of FI hosted in wolframite. Pure water (0 ℃) in synthetic FI and potassium bichromate (398 ℃) were used for calibration. The accuracy of measurements is in the order of ±0.1 ℃ for final melting temperatures of ice and ±2 ℃ for homogenization temperatures. FI microthermometry analysis was carried out at the State Key Laboratory for Mineral Deposits Research, Nanjing University.

5.3. Fluid inclusion LA-ICP-MS analysis

Elemental compositions of fluid were determined by LA-ICP-MS on selected FIs hosted by wolframite, scheelite and quartz. LA-ICP-MS analyses were carried out at the inclusion LA-ICP-MS lab in Nanjing University using a Coherent GeolasHD laser system coupled to a Perkin Elmer 350X quadrupole ICP mass spectrometer. Considering the absence of infrared optical camera in the laser ablation system, precisely locating of wolframite-hosted FIs is critical prior to analysis. Positioning

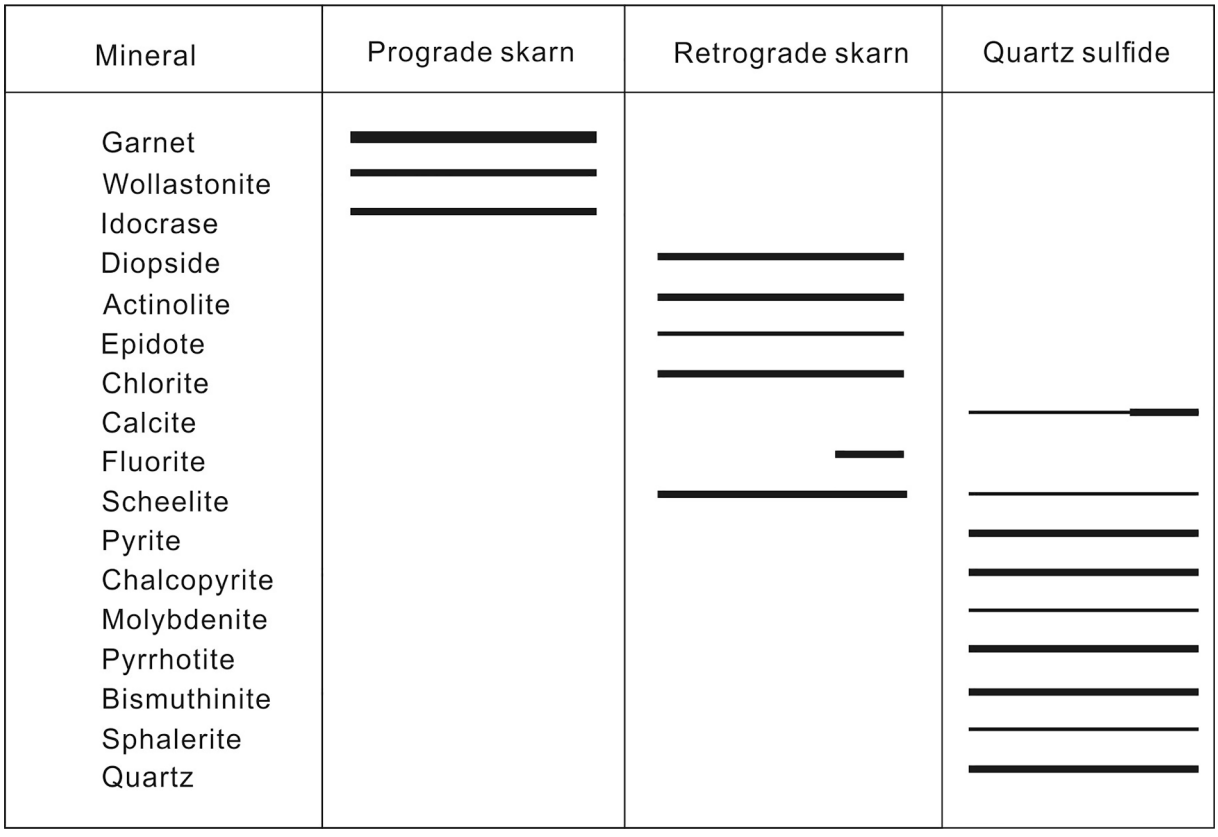

Fig. 6. Paragenetic sequences of minerals in the Yuxin section.

procedure and instrumental setup protocols described in Pan et al., (2019) was applied for all analysis. An energy density of 10 J/cm^2 and a pulse frequency of 10 Hz were used for quartz ablation. Meanwhile, a stepwise increase of beam size was applied to avoid quartz decrepitation. For wolframite and scheelite, ablation was carried out using a laser pulse frequency of 15 Hz, energy density of 5 J/cm^2, and fixed spot size that is slightly larger than the target fluid inclusion. The standard reference material NIST 610 and an in-house scapolite Sca-17 (Seo et al., 2011) were used as the external standards, and apparent NaCl equivalent salinities obtained from microthermometry was used to calculate the Na concentration which is used as internal standard. A group of isotopes listed in Supplemental Table S1 were measured for each fluid inclusions and external standards. Due to matrix effect, elements that present in considerable concentrations in certain host minerals cannot be determined in fluid inclusion.

The SILLS software package was used to process the raw data of all fluid inclusions and the host minerals (Guillong et al., 2008). To remove the host interference on the fluid inclusion signal, W, Ca and Si were used as matrix-only tracers for wolframite, scheelite and quartz, respectively. The limits of detection (LODs) of measured elements were calculated using the 3σ standard deviation of the background intensities (Heinrich et al., 2003; Pettke et al., 2012). To ensure the reliability of the reported values, signal peaks of each fluid inclusion were double checked and the outliers which commonly do not correspond to true signal peaks were reported as LODs. Average elemental concentration with uncertainties of ±1σ standard deviation were calculated using all obtained values in each fluid inclusion assemblage. The scheelite composition were also obtained using the matrix signal of corresponding fluid inclusion analysis.

6. Analysis results

6.1. Fluid inclusion petrography

All the microanalyses were focused on FIs that are either trapped along growth zones of host minerals or captured as trails that are truncated by further crystal growth, indicating primary or pseudosecondary origin based on the criteria of Goldstein (2003). Secondary FIs were not included in our study as their representativeness is ambiguous. Most FIs measured in our study occur in fluid inclusion groups or clusters containing similar liquid-to-vapor ratios, namely fluid inclusion assemblage (FIA) (Goldstein and Reynolds, 1994). Fluid inclusions in each FIA exhibit similar heating and freezing behavior, indicating that they were trapped from an identical fluid under similar conditions (Fall and Bodnar, 2018). Given their phases present at room temperature, two-phase aqueous inclusion is the only fluid inclusion type that were identified in wolframite, scheelite and quartz of this study. According to the host minerals, detailed petrographic descriptions of the studied FIAs are presented below.

Primary FIs in wolframite (Pw) contain liquid and a vapor bubble that occupies 20 to 30 vol% of the inclusion at room temperature (Fig. 7A, B). These inclusions typically show shapes of negative wolframite crystal or rounded rectangle, and they were identified as primary as they were trapped along euhedral growth zones of wolframite (Fig. 7A, B). Several selected quartz crystals associated with wolframite show growth zone decorated by small muscovite crystals (Fig. 7C) as described in Pan et al. (2019). Numerous FI trails in quartz (Wq) were truncated by the growth zones and thus indicate pseudosecondary FIAs (Fig. 7C). These fluid inclusions with negative crystal of the quartz has filling degrees between 20 and 30% (Fig. 7D). Consistent with our previous observations (Pan et al., 2019), the studied quartz crystals all show later paragenetic sequence to the coexisting wolframite

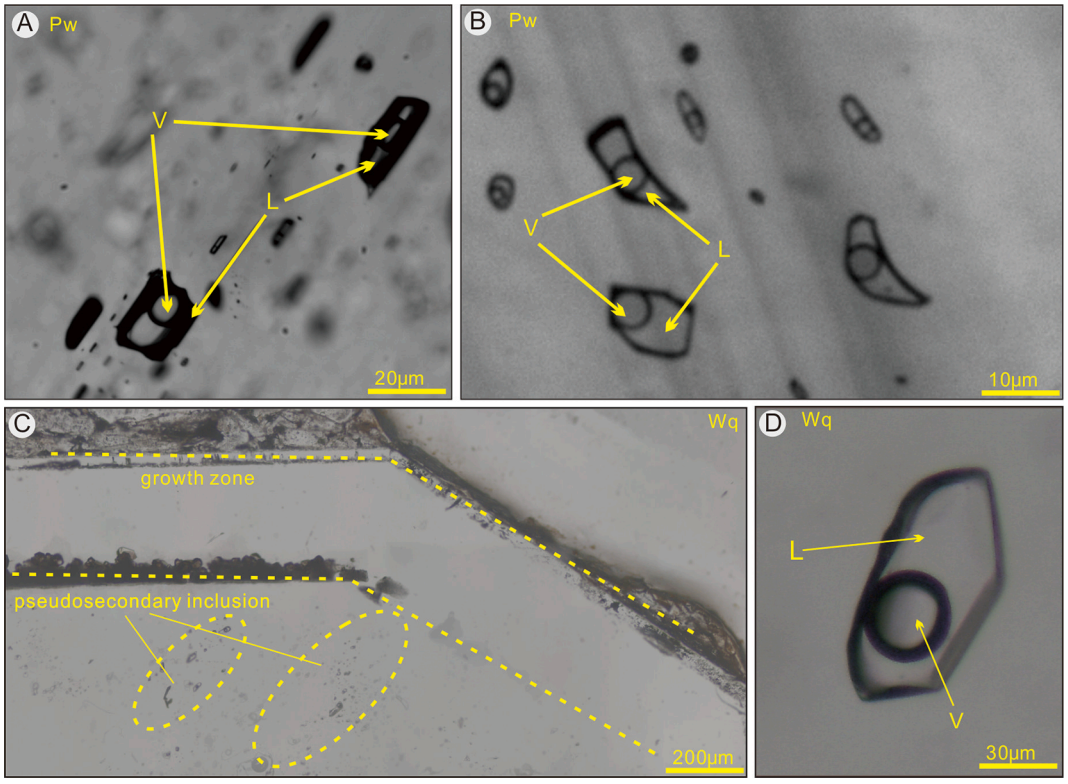

Fig. 7. Representative photomicrographs of fluid inclusions hosted in wolframite and quartz from wolframite quartz vein. A-Fluid inclusion assemblage containing Pw fluid inclusions along growth zones of wolframite, indicating a primary origin. B-Flat Pw fluid inclusions were trapped along euhedral growth zones of wolframite. C-Pseudosecondary Wq fluid inclusion assemblage truncated by growth zone. D-Wq fluid inclusion with negative crystal of the quartz. Abbreviations: Pw = Primary FIs in wolframite, Wq = Primary FIs quartz associated with wolframite, V = vapor, L = liquid.

and the quartz-hosted fluid inclusions therefore represent the hydrothermal fluids trapped after major wolframite deposition in veins.

Both primary and secondary inclusions occur in scheelite-1 (Fig. 8A). The common occurrence of secondary FI trails suggests that scheelite-1 has been affected from late stages hydrothermal events. In contrast to secondary FIs, primary FIs in scheelite-1 (Ps1) are commonly larger in size and trend to form isolated groups. Due to the lack of well-defined growth texture in these small-grained scheelite crystals, it is sometimes difficult to distinguish between primary and pseudosecondary FI groups. Nevertheless, these fluid inclusions are both interpreted to represent the ore-forming fluids of scheelite-1. Ps1 inclusions generally contain 25–30 vol% of bubble at room temperature. The size of Ps1 can vary between 5 μm up to 25 μm in some individual FIAs (Fig. 8B). Primary FIs in scheelite-2 (Ps2) are mostly randomly distributed in the cores of scheelite grains (Fig. 8C), with few trapped as trails that are limited within crystal grains, indicating pseudosecondary in origin (Fig. 8D). These inclusions typically range in shapes from negative scheelite crystal to rounded rectangle and contain 20–25 vol% of vapor at room temperature (Fig. 8C). The quartz grains associated with scheelite-2 in sulfide stage veins are less euhedral than those collected from cavities of wolframite-quartz veins, and thus do not show obvious growth textures as presented in Fig. 7C. However, FI (Sq) trails entrapped along limited cracks within the crystals were recognized as pseudosecondary in origin (Fig. 8E). The quartz-hosted fluid inclusions have variable sizes in diameter (10–40 μm) and generally exhibit negative crystal or irregular shapes (Fig. 8F). It is worth to note that in the Yuxin section, the fluid inclusions recorded in scheelite 1 predate scheelite 2 and quartz.

6.2. Microthermometry

All Pw FIs homogenize to liquid between 289 and 313 °C, with a mean of 299 °C. Most Pw inclusions have final melting temperatures between −2.6 and −5.2 °C with a mean value of −4 °C. This indicates a salinity range of 4.3 ~ 8.1 wt% NaCl eq. For those inclusions in quartz associated with wolframite, final melting occurred between −2.4 and −3.8 °C, suggesting variable salinity of approximately 4.0 ~ 6.2 wt% NaCl eq. Vapor disappearance occurred between 234 and 273 °C. First melting of five large FIs were observed to have occurred at −21.3 and −21.6 °C, suggesting a NaCl dominated salt-H_2O system.

During heating, the vapor bubbles in Ps1 homogenize to the liquid at Th ranging from 308 to 333 °C. Calculated salinities derived from ice melting temperatures range between 6.9 and 8.2 wt% NaCl eq. The Ps2 homogenize into the liquid phase at temperatures between 270 and 286 °C and have salinities of 5.7–6.3 wt% NaCl eq. Homogenization temperatures of Sq FIs vary from 255 to 276 °C and salinities range between 4.6 and 5.6 wt% NaCl eq. It is apparent that the Ps2 display much lower temperatures than Ps1, but have similar temperature to those Sq FIs.

The microthermometric data for the FIAs in the Dayanmen and Yuxin sections has been plotted on Fig. 9A, B and C, respectively. The Wq FIAs clearly show much lower Th than coexisting wolframite-hosted FIAs (Fig. 9B) and it is consistent with the fact that quartz precipitation is later than wolframite. The slightly variable salinities recorded in both wolframite and Wq FIAs likely reflects their minor but variable CO_2 contents as has been elaborated previously (Pan et al., 2019). However, the continued decrease in both homogenization temperature and salinity in FIAs from retrograde stage to sulfide stage (Fig. 9C) likely indicate meteoric water mixing in the skarn system.

6.3. Fluid composition

The elemental composition of 139 individual FIs was analyzed by LA-ICP-MS (73 from wolframite-quartz vein and 66 from scheelite-skarn). Selected elemental compositions are reported in Supplemental Table S1 and plotted in Figs. 10 to 13. FIs in both wolframite and scheelite ore sections have Na as the major cation, with K in Pw and Ps1 inclusions being another major cation. The dataset does not present Ca, Fe, Cu, Zn and Pb and is limited for Sr, W and Mn. This is partly due to the matrix effect of wolframite and scheelite and partly because in many FIs these elements were below their limits of detection. Other abundant

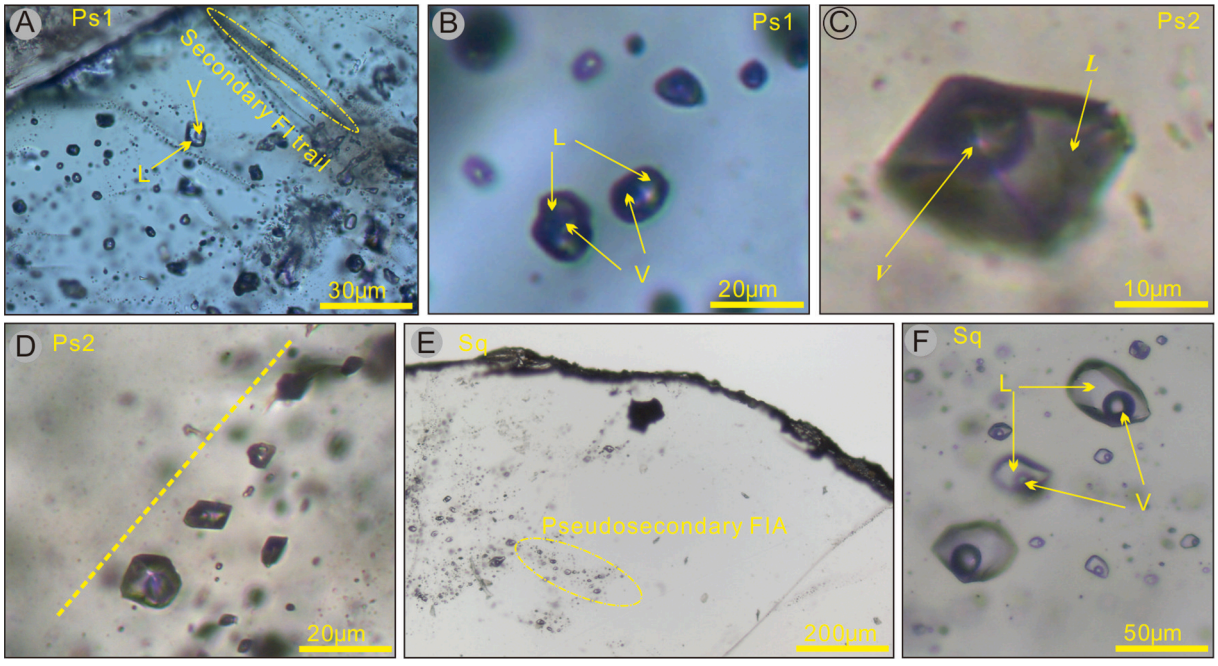

Fig. 8. Photomicrographs of typical fluid inclusions in scheelite and quartz from skarn scheelite. A-Ps1 fluid inclusions with a secondary fluid inclusion assemblage trail. B-Ps1 Fluid inclusion assemblage hosted in scheelite 1. C-Typical isolated regular Ps2 fluid inclusion. D- Ps2 fluid inclusions trapped as trails that are limited within crystal grains, indicating pseudosecondary in origin. E-Sq Fluid inclusions on a pseudosecondary trail in a quartz crystal associated with scheelite. F-Typical Sq fluid inclusions in quartz. Abbreviations: Ps1 = primary FIs in scheelite-1, Ps2 = primary FIs in scheelite-2, Sq = fluid inclusions in quartz grains associated with scheelite-2. V = vapor, L = liquid.

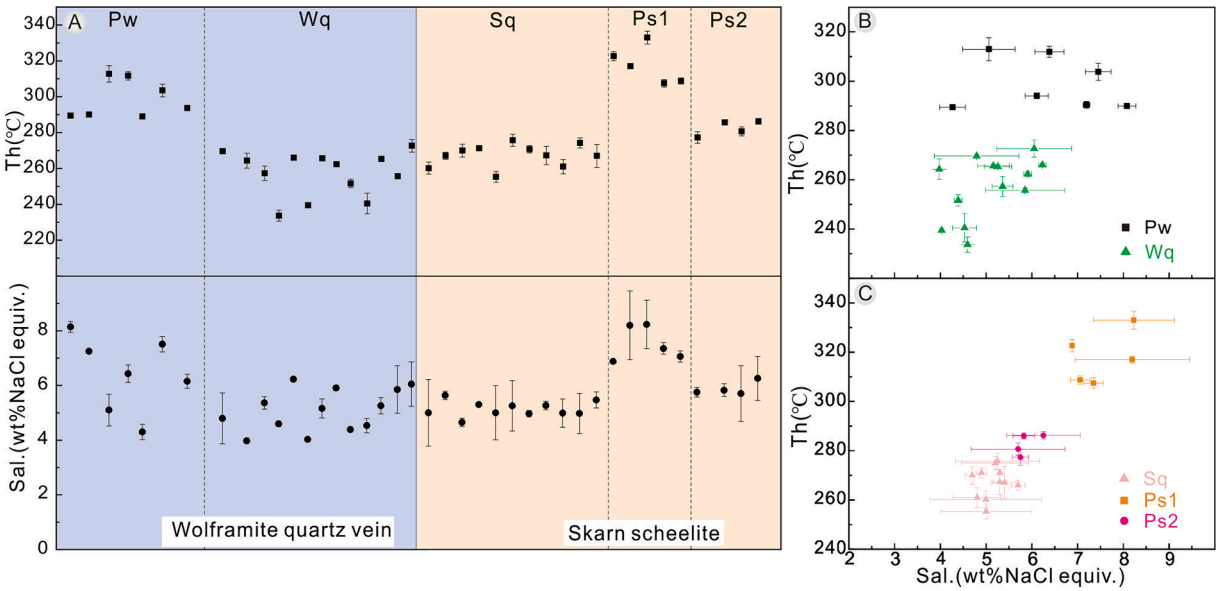

Fig. 9. A-Plots for homogenization temperature, salinity of fluid inclusion assemblages in different minerals of vein and skarn mineralization in the Yaogangxian W deposit. Plot of homogenization temperature versus salinity of fluid inclusion assemblages for wolframite quartz vein(B) and skarn scheelite (C). Pw = Primary FIs in wolframite, Wq = Primary FIs quartz associated with wolframite, Ps1 = primary FIs in scheelite-1, Ps2 = primary FIs in scheelite-2, Sq = fluid inclusions in quartz grains associated with scheelite-2.

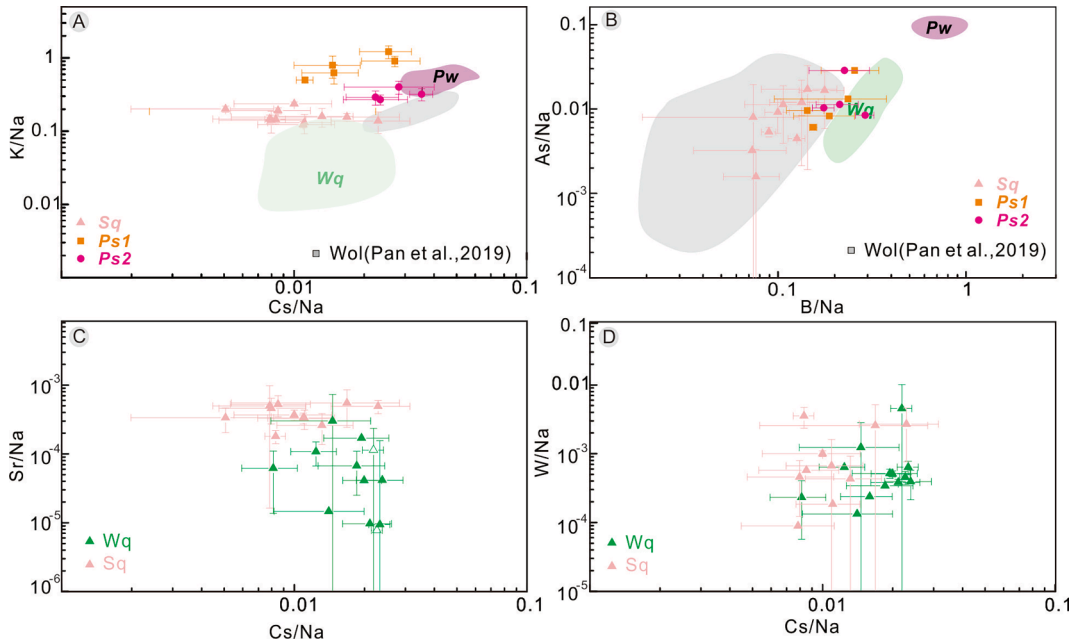

Fig. 10. Binary plots fluid inclusion compositions in the Yaogangxian W deposit. logarithmically plotted Cs/Na vs. K/Na (A), B/Na vs. As/Na (B), Cs/Na vs. Sr/Na (C), Cs/Na vs. W/Na (D) subtracting the influence of the salinity and showing element contents in fluid of diverse W mineralization style. Wol = Fluid inclusions in wolframite.

elements that were detectable throughout all measurements were Rb and Cs and B with average values of 156 ppm, 399 ppm, and 5204 ppm respectively. Cl and As were also determined in most fluid inclusions.

As plotted in Fig. 10A, Ps1 FIAs showed the highest K concentrations (9113.3–23530.4 ppm) in all measured inclusions. Almost all the high values of As and B content are recorded in the Pw FIs (Fig. 10B). The content of Sr in fluid recorded in quartz from the Yuxin section is significantly higher than that in the Dayanmen section (Fig. 10C). W contents in quartz-hosted FIs can vary over an order of magnitude within single FIA, but the overall values of W/Na from the Dayanmen and Yuxin section fall in a similar region (Fig. 10D).

Comparison of average chemical compositions of FIs in different minerals are plotted in Fig. 11. The Pw inclusions show higher X/Na ratios of nearly all elements compared to FIs in later coexisting quartz (Fig. 11A), similar to the chemical evolution trend between wolframite- and late-stage quartz-hosted FIs in our previous study (Pan et al., 2019). In particular, there is a strong decrease of K, Li, Rb and As from Pw to quartz-hosted FIs, indicating muscovite and arsenopyrite deposition. In the Yuxin ore section, Ps1 and Ps2 inclusions show similar chemistry for most elements except for K, which is markedly lower in Ps2 (Fig. 11B). The average chemical compositions of the Sq FIs is characterized by generally lower X/Na ratios of most elements (Fig. 11C). The

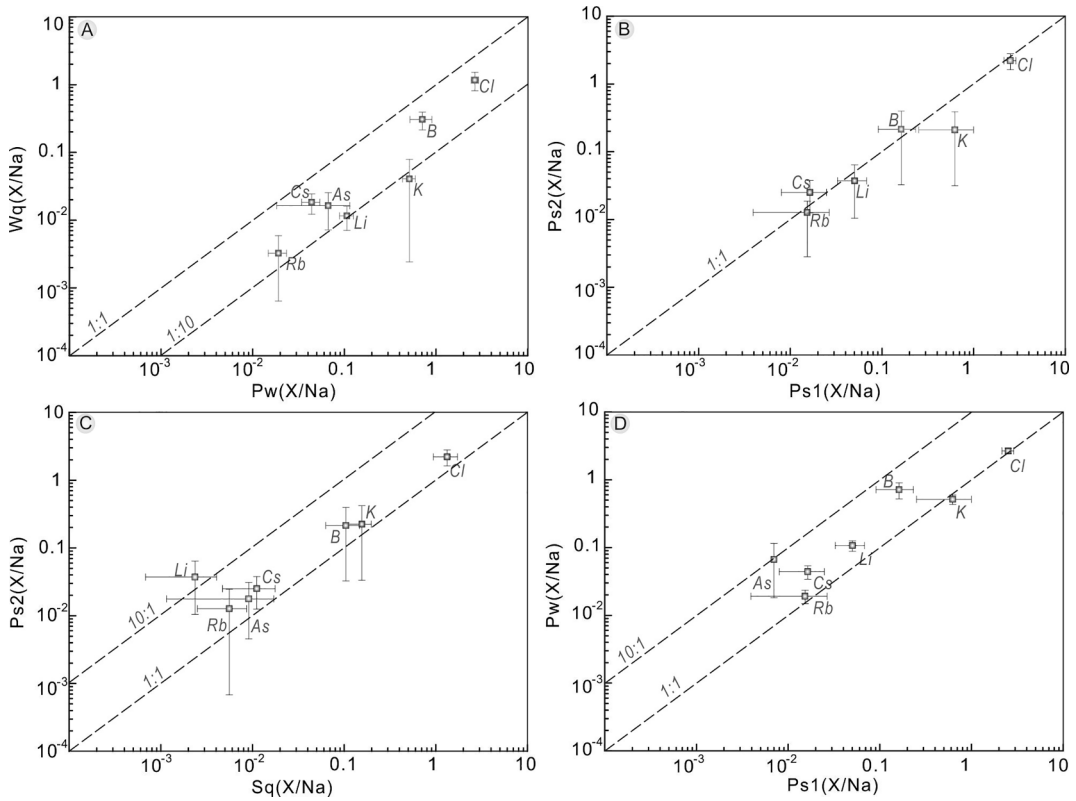

Fig. 11. Comparison of fluid chemistry between quartz and diverse ore minerals. primary inclusions in wolframite vs. coexisting quartz (A), primary inclusions in scheelite 1 vs. scheelite 2 (B), primary inclusions in scheelite 2 vs. coexisting quartz (C), primary inclusions in wolframite vs. scheelite 1 (D). In each diagram, only those elements detected in both fluid inclusion types are plotted.

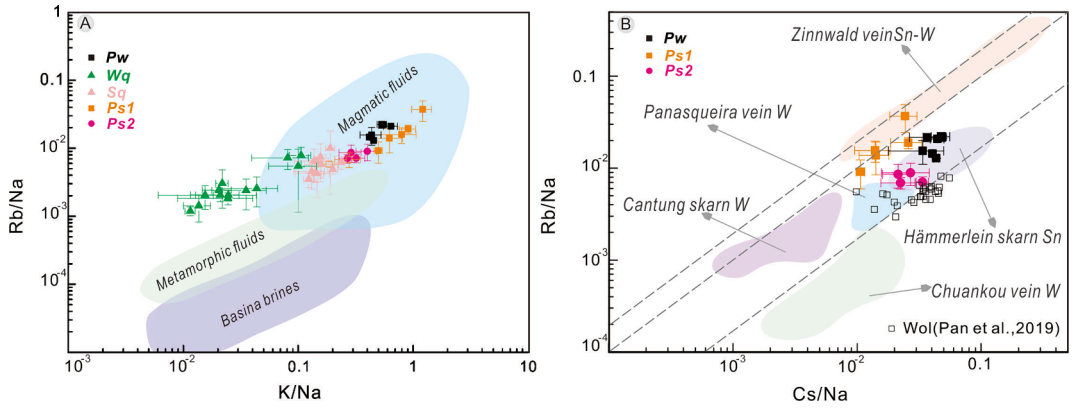

Fig. 12. A-K/Na versus Rb/Na of fluid inclusion hosted in different minerals and the constructed domains of different fluid sources (modified after Han et al. 2023 and references therein). B-Binary plots of Rb/Na versus Cs/Na of fluid inclusions and comparison with other vein-type and skarn-type W-Sn deposits worldwide (for data sources, see study: Panasqueira-Lecumberri-Sanchez et al., 2017; Cantung-Hämmerlein-Korges et al., 2018; 2020; Cantung-Legros et al., 2020; Li et al., 2022).

compositions of the earliest ore-forming fluids obtained in both W ore sections are generally similar except for that the ore-forming fluids responsible for wolframite formation show higher B and As contents (Fig. 11D), which is probably consistent with the fact that arsenopyrite and tourmaline in the wolframite-quartz vein systems are much more abundant than the scheelite-skarn.

7. Discussion

7.1. Fluid source responsible for wolframite and scheelite mineralization

It is widely accepted that the ore-forming fluids of vein type tungsten deposits are derived from granitic magmatism (Kelly and Rye, 1979; Hulsbosch et al., 2016; Korges et al., 2017; Li et al., 2020). For skarn scheelite system, different views exist on the main source of the hydrothermal fluid. Most scholars suggest that the ore-forming fluid carrying metals is mainly magmatic hydrothermal fluid, (Fonteilles et al., 1989; Tornos et al., 2008; Oyunjargal et al., 2019), with variable amount of meteoric water input in the late stage (Lu et al., 2003; Poblete et al., 2021). Ishihara et al., (2003) also considered the strata-sourced fluid may play a key role in the formation of scheelite-skarn in addition to magmatic sourced fluids. According to the study of $CO_2 \pm CH_4 \pm N_2$ fluid inclusions in vesuvianite and C-O isotopic analysis, a metamorphic origin for hydrothermal fluids in the Los Santos skarn was proposed (Tornos et al., 2001; Timón et al., 2007). To trace the ore-forming fluid source in the Yuxin ore section, fluid inclusion composition data was

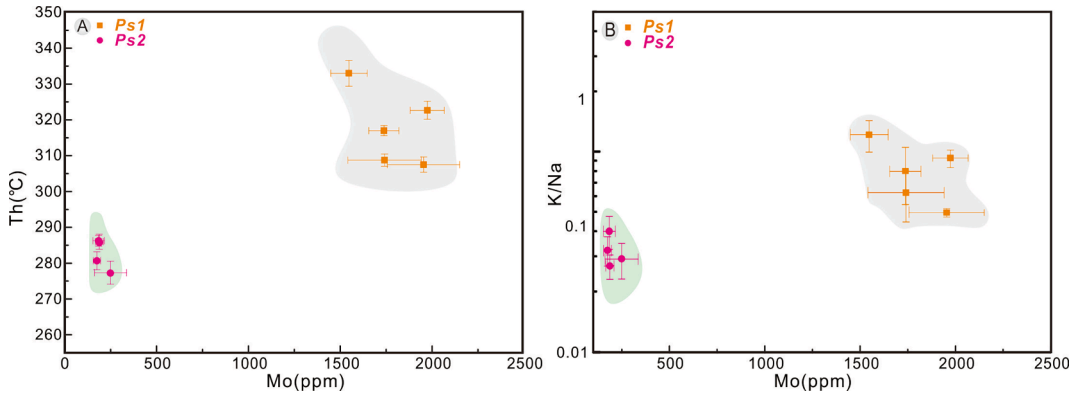

Fig. 13. A-Correlations of Mo concentration obtained by *in-situ* mineral analysis and 2 vs. Th for fluid inclusion; B- logarithmically plotted K/Na vs. Mo. The Mo concentrations were obtained by *in-situ* mineral analysis.

plotted in comparison with typical domains constructed for magmatic fluids, metamorphic fluids and basinal brines worldwide (Fig. 12A). The fluid composition obtained from scheelite and quartz in the Yuxin ore section all fall into the magmatic fluid domain together with those obtained from wolframite in the Dayanmen ore section, suggesting a clear magmatic source without significant involvement of metamorphic or basinal fluids. Addition of meteoric water cannot be testified here but it is evident from microthermometry data shown in Fig. 9C. The fluids recorded in quartz coexisting with wolframite show lower Rb/Na and K/Na ratios compared with W mineralizing fluids and are biased from typical magmatic fluids. This trend together with the similar trend displayed between Ps1 to quartz-hosted FIs in the scheelite-skarn are interpreted to reflect muscovite or sericite deposition during fluid evolution (Pan et al., 2019), and they are consistent with our paragenetic observations (e.g., Fig. 4C & Fig. 5G).

At Yaogangxian, fluid inclusions from wolframite and coexisting quartz has been previously investigated in details (Pan et al., 2019), and the study shows that FIs hosted in both wolframite and coexisting quartz may provide important information on the ore-forming fluids. However, the studied samples in our previous study were obtained from very high level (1200 m above sea level), which is relatively distant from the granitic intrusion and the roots of ore veins. Considering the possible chemical changes of fluids along it upwelling, this study focused on the vein samples collected from the deepest level (26 level) which likely recorded early magmatic fluids that may be physically and chemically less modified. Although ore-forming fluids of the two W mineralization styles in Yaogangxian are both controlled by magmatism, a major debate centers on whether the two mineralization share an identical parental granitic magma. For example, Zhu et al. (2015b) proposed that two distinct granite phases formed wolframite-quartz vein and skarn scheelite, respectively. In contrast, Xu, (1957) emphasized that the divers W mineralization styles in Yaogangxian were sourced from an individual magmatic hydrothermal system but were controlled by different wall rocks. Considering the strong incompatibility of alkali metal elements such as Rb and Cs in hydrothermal process, Cs/Rb ratios can be used to trace the diversity of the magmatic fluid source (Klemm et al. 2008; Korges et al. 2017; Pan et al., 2019; Han et al., 2023). Here, the fluid composition obtained from wolframite and scheelite are plotted in the Rb/Na and Cs/Na diagram and are compared with other vein-type and skarn-type W-Sn fluids from literatures (Fig. 12B). It is shown that the Cs/Rb ratios of fluids in both ore sections are concentrated in a narrow range. Considering the Rb contents can be affected by muscovite deposition as discussed above, the Pw and Ps1 fluids are so far the best record of the initial magmatic fluid signatures, and their chemical consistence clearly indicates an identical magmatic source (Fig. 12B). Combining these results with the close spatial–temporal affinity between the Yaogangxian granite and the two mineralization styles and their consistent geologic age (Li et al., 2011; Li et al., 2020), we speculate that a consistent deep origin magma dissolved W-rich fluid responsible for both vein and skarn type mineralization.

7.2. Precipitation mechanism of wolframite and scheelite

Recent fluid inclusion and isotopic studies have proposed several precipitation mechanisms for wolframite deposition. For example, based on the statistical analysis of microthermometry data from wolframite-hosted fluid inclusions in several vein-type W deposits in South China, simple cooling of fluids is proposed as an important mechanism to trigger wolframite precipitation (Ni et al., 2015; Li et al., 2018; Chen et al., 2019). Korges et al. (2017) proposed that fluid boiling induced by decompression plays a key role in wolframite precipitation in quartz veins at Zinnwald. Mixing between magmatic fluid and meteoric water is also thought to result in wolframite precipitation, as supported by the findings that multiple fluids are involved within a single deposit (Legros et al., 2019). Recent studies of fluid chemistry and wall rock alteration in Panasqueira and Chuankou W deposits also provide evidences supporting fluid-rock interaction as a main mechanism for wolframite deposition (Lecumberri-Sanchez et al., 2017; Li et al., 2022a; Li et al., 2022b). For scheelite-skarn, fluid boiling was a possible mechanism for scheelite precipitation associated with retrograde stage (Sanchez et al., 2009, Soloviev and Kryazhev, 2019; He et al., 2022), while the mixing of magmatic fluid with meteoric water is generally thought to be the main process for quartz-sulfide stage mineralization (He et al., 2022). Additionally, based on radiogenic and stable isotope signatures and REE contents of the scheelite, Tornos et al. (2008) proposed that scheelite only precipitated by replacement of marble where Ca were attained. Multiple fluid processes can also jointly trigger scheelite precipitation within the same deposit. For example, Soloviev and Kryazhev (2017) suggested that fluid immiscibility and cooling, combined with Ca enrichment in the fluid collectively triggered significant scheelite precipitation in the Skrytoe scheelite-skarn deposit in Russia. In summary, controversies exist on precipitation mechanism for both wolframite and scheelite.

In Yaogangxian, the fluid processes forming coexisting wolframite and quartz has been studied in sufficient detail on samples collected at the upper part of the vein systems (Pan et al., 2019). Our previous results show that the ore-forming fluid responsible for wolframite deposition is mainly characterized by significant loss of CO_2 and CH_4 and deprivation of B, As, and S, suggesting that the loss of volatiles due to fluid immiscibility is one of the important fluid processes concurrent with wolframite precipitation. To present a more comprehensive constraint on the ore-forming fluid precipitating wolframite at Yaogangxian, our previous data is integrated and compared with the newly obtained data in Figs. 10 and 11. It is obvious that the Pw inclusions in wolframite of the current study exhibit strong enrichment of B and As (Fig. 10B), and to a lesser extent K (Fig. 10A) and Rb (Fig. 12B). Given that the studied

wolframite was collected from the root of vein systems whereas our previously studied wolframite was collected at the distal part, the lowered K and Rb contents in the ore-forming fluids clearly indicate muscovite deposition during fluid upwelling, and this is in good accordance with the geological fact that early stage muscovite formation is pervasively associated with wolframite mineralization in veins. Because wolframite attached to the vein wall is one of the earliest minerals formed in the depositional sequence, formation of arsenopyrite and tourmaline during early-stage fluid-rock interaction (Fig. 4C) best explain the lowered As and B contents in the early-stage ore-forming fluids during its ascending. The relatively higher As and B contents in deep ore-forming fluid may also suggest absence of intensive fluid immiscibility (Pan et al., 2019), which is reasonable considering higher fluid pressure in the deep. These new knowledges imply that fluid-rock interaction may have played a previously neglected role in wolframite deposition at Yaogangxian, but further investigations on the chemical changes in wall rock and the property of fluid prior to wolframite deposition are needed to clarify this mechanism. However, it is important to note that the early-stage ore-forming fluid from scheelite at the Yuxin section also display lowered As and B contents compared to the deep ore-forming fluid for wolframite (Fig. 10B & 11D). Given that alterations involving arsenopyrite and tourmaline are absent in prograde to retrograde skarn, the low As and B contents in scheelite fluids suggest that boiling may have occurred at early skarn stage, which is commonly observed in skarn deposits (Sanchez et al., 2009; Yang et al., 2017).

Fluid mixing between a high temperature, high salinity magmatic fluid and a low temperature, low salinity meteoric water is commonly invoked as an efficient mechanism for ore deposition in skarn deposits (Brown and Essene, 1985; Layne and Spooner, 1991; Singoyi and Zaw, 2001; Lu et al., 2003). Our microthermometry data suggest a clear involvement of meteoric water mixing during the scheelite ore forming stages (Fig. 9C). This process can be further testified by comparison with previous stable isotopic composition (Wang et al., 2014). In the retrograde stage of skarn, the addition of meteoric water is a common phenomenon. For example, the fluids responsible for stockwork ore in the giant Shizhuyuan W-Sn-Mo-Bi deposit are proposed as mixtures of magmatic and meteoric water (Lu et al., 2003). In the Kara W deposit in Tasmania, the mixing between low salinity meteoric water and high salinity magmatic fluid causes changes in the physical and chemical conditions of ore-forming fluid, and is suggested as a main factor triggering large-scale scheelite precipitation (Singoyi and Zaw, 2001).

7.3. Mineralizing condition for scheelite-skarn system

In scheelite-skarn deposits, massive precipitation of scheelite may occur in prograde metasomatic stage (Zaw and Singoyi, 2000; Lu et al., 2003; Oyunjargal et al., 2019) and/or with considerable amount in the retrograde stage (Kwak and Tan, 1981; Sanchez et al., 2009). Based on field and petrographic relationships, two stages of scheelite were identified in the Yuxin ore section, i.e. scheelite-1 (retrograde stage skarn) and scheelite-2 (quartz-sulfide stage). Our fluid inclusion results show that the two stages of scheelite have distinctly different fluid Th and salinity, but share very similar trace element compositions (Fig. 11B). K and Rb contents are the only exceptions which are slightly lower in scheelite-2 fluids compared with scheelite-1 (Fig. 10B & 12A). As discussed above, this can be attributed to significant sericitization at quartz-sulfide stage. It has been proved that replacement of prograde skarn minerals such as garnet by retrograde skarn can release Ca necessary to form scheelite (Newberry, 1983). This may explain the replacement of garnet by scheelite grains in the retrograde stage (Fig. 5D). On the other hand, the large gap of temperature between two scheelite stages may suggest that scheelite deposition can occur in a wide range of temperature condition (270–340 °C).

Scheelite ($CaWO_4$) crystal structure has two unique cation sites, in which alkaline earths, alkalis, and highly charged, smaller cations are easy accommodated (e.g., W^{6+}, Mo^{6+}, As^{5+}, Nb^{5+},Na^{+}) (Raimbault et al., 1993; Poulin et al., 2016). Trace element composition of scheelite varies as a function of the origin and physicochemical conditions of hydrothermal fluids from which it precipitates and thus is used to reflect ore-forming conditions (Poulin et al., 2016; Miranda et al., 2022). In particular, Mo in scheelite is used to quantitatively reconstruct the changing physicochemical conditions during ore formation (Song et al., 2014; Miranda et al., 2022). Under oxidizing conditions, Mo would migrate as Mo^{6+} rather than Mo^{4+}, and thus would be easy to substitutes W^{6+} in scheelite (Hsu, 1977). In the Yuxin section, the LA-ICP-MS results of scheelite formed in retrograde skarn and quartz-sulfide vein stage give diverse Mo contents. Scheelite-1 show an average Mo concentration of 1779 ppm, whereas scheelite-2 has an average Mo concentration of 237 ppm (Fig. 13). The high Mo concentrations in scheelite-1 indicate a relatively oxidizing environment in retrograde skarn stage compared to scheelite-2 in sulfide stage. This finding is also supported by the occurrence of abundant sulfide minerals such as pyrrhotite in the sulfide-quartz vein, indicative of a relatively reduced environment (Fig. 5J, K and L). It should be noted that earlier deposition of scheelite may also cause Mo depletion in late stage. The trend of decreasing Mo contents in scheelite from early to late was also revealed in the Zhuxi and Weondong W-skarn deposits (Yuan et al., 2019b; Choi et al., 2020). Combining the composition of the fluids, we propose that a high temperature, high K and oxidizing fluid and a low temperature, low K and relatively reducing fluid are responsible for the precipitation of scheelite-1 and scheelite-2, respectively (Fig. 13). Considering that more than 90% of the scheelite in the Yuxin section occur as scheelite-1, we suggest that the Yuxin skarn scheelite was formed under higher temperature and relatively oxidized condition. It should not be ignored that W mineralization at sulfide stage also holds economic significance, indicating that the oxygen fugacity variation does not behave as the dominate control for scheelite precipitation (Brown and Essene, 1985; Choi et al., 2020). It has been shown that economically valuable scheelite can be precipitated under both oxidizing and reducing conditions. For example, the reduced skarn in the MacTung W deposit from the northeastern Canadian Cordillera (Dick and Hodgson, 1982) and the oxidized skarn in the Weondong W-skarn deposit, South Korea (Choi et al., 2020).

7.4. Genetic model for the Yaogangxian W deposit

In the Yaogangxian deposit, Xu (1957) investigated, through geological mapping and mineralogical study, the importance of structural and stratigraphic controls on different W mineralization styles. Despite a genetic link between the two W mineralization styles has been assumed by Xu (1957), no valid evidence has been provided until recent geochronological data being reported (Li et al., 2011; Li et al., 2020). Li et al., (2020) obtained the cassiterite age (158 ± 1.9 Ma) in wolframite-bearing quartz veins, which is consistent with molybdenite Re–Os age (160 ± 3.3 Ma) in skarn W mineralization style (Li et al., 2011). Recent geochronological studies have shown that the lifespan of granite-related W-Sn hydrothermal ore system is as short as several hundreds of Ka, and the time for mineralization can only account for less than 10%, i.e., in the scale of several millennium or less (Li et al., 2023). This implies that the reported mineralization ages at their current analytical precision do not necessarily demonstrate the genetic link between the two mineralization. Nevertheless, our fluid inclusions data does reveal a magmatic fluid identical in chemistry is responsible for the formation of both W mineralization styles at Yaogangxian. Based on this conclusion and previous geological and geochronological studies, a metallogenic model of the coupled wolframite-quartz vein and scheelite-skarn mineralization has been establish in Fig. 14.

Tungsten exists in hydrothermal fluids mainly in the +6-valence state and readily forms tungstate species in hydrothermal fluids, which forms wolframite or scheelite by combining with Fe^{2+}, Mn^{2+} and Ca^{2+} (Wood and Samson, 2000; Wang et al., 2019). There is a general consensus that W for wolframite and scheelite formation mainly

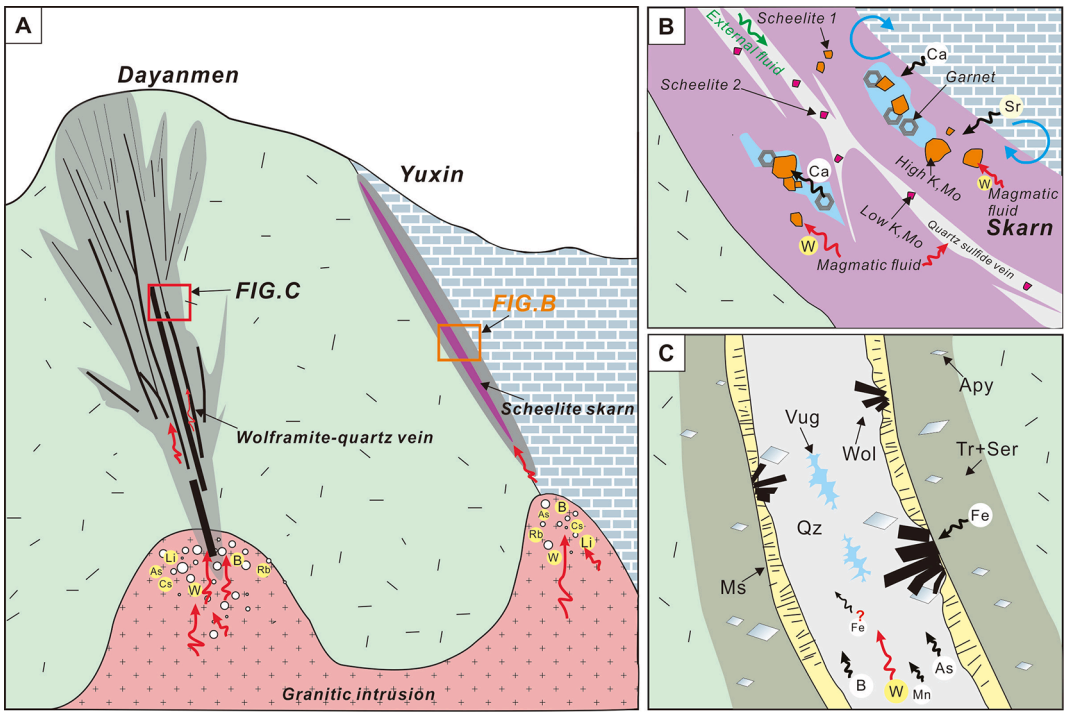

Fig. 14. Schematic metallogenic model of the coupled wolframite-quartz vein and scheelite-skarn mineralization at the Yaogangxian W deposit. A-An identical magmatic fluid source is responsible for vein and skarn type W mineralization. B- Two types of scheelite formed with different fluid compositions and mineralizing conditions. Addition of Ca from the host carbonate and mixing with external meteoric water caused scheelite precipitation. C- wolframite mainly formed early in the depositional sequence followed by quartz and other minerals. Alteration in the quartzofeldspathic metasedimentary wall rock likely provide in part Fe which is necessary for wolframite deposition. Abbreviations: Wol = wolframite, Qz = quartz, Ms = sphalerite, Apy = arsenopyrite, Tr = tourmaline, Ser = sericite.

originates from the granitic magma (Lecumberri-Sanchez et al., 2017; Li et al., 2020), whereas the Fe and Ca can come from magma (Carocci et al., 2020) and/or the surrounding rocks (Lecumberri-Sanchez et al., 2017; Li et al., 2022). The common association between scheelite mineralization and Ca-rich host rocks worldwide strongly suggest that the Ca necessary for scheelite formation originates largely from the host rock, and it is even valid in non-skarn systems. For example, the rock-buffered activity of Ca from Ca-rich metavolcanics in the Sisson Brook W-Cu-Mo deposit is responsible for scheelite deposition (Nast and Williams-Jones, 1991). Similarly, the Ca-rich sandstone provide the source of Ca for the precipitation of scheelite in the Chuankou W deposit (Li et al., 2022). Therefore, we propose that the Ca responsible for the precipitation of scheelite in the Yuxin section is primarily contributed by carbonate (Fig. 14B).

However, the origin of Fe necessary for wolframite formation in veins remain debated. For the Panasqueira W deposit, depends on the availability of Fe in fluid and host rock, Lecumberri-Sanchez et al. (2017) suggest that the host rock contributes the Fe required to precipitate wolframite. In contrast, Carocci et al. (2020) proposed that late magmatic source fluids carry the Fe required for wolframite deposition. The absence of parent ore-forming fluid composition means that the present study cannot confirm the origin of Fe necessary for wolframite deposition, which may partly come from alteration of the host rock, or come directly from the magma (Fig. 14C).

8. Conclusions

(1) The chemical compositions of the ore-forming fluids obtained by LA-ICP-MS suggest that the fluids responsible for successive ore and gangue mineral (wolframite, scheelite, quartz) precipitation in both wolframite-quartz veins and scheelite-skarn at Yaogangxian can be traced back to an identical magmatic fluid source. Formation of diverse W mineralization styles is likely controlled by different host lithology and fluid processes. The fluid responsible for scheelite-skarn exhibits lower As and B contents than wolframite-quartz veins suggest that boiling may have occurred at early skarn stage.

(2) Fluid inclusion data from coexisting wolframite and quartz collected at the root of the vein displays a chemical evolution similar to our previous findings obtained from samples at the tip of the vein. The ore-forming fluid entrapped at deep show higher K, B and As contents than those entrapped in wolframite at shallow part of the vein. This likely suggests muscovite, tourmaline and arsenopyrite deposition during fluid upwelling and may also indicate absence of intensive fluid immiscibility in the deep. These new knowledges imply that fluid-rock interaction may have played a previously neglected role in wolframite deposition at Yaogangxian, but further investigation is still needed to clarify this mechanism.

(3) In skarn-type W mineralization, two generations of hydrothermal scheelite were identified, including scheelite-1 from retrograde stage skarn and scheelite-2 in quartz-sulfide stage. Microthermometry reveals that constant injection of meteoric water is evident between two mineralization stages. Both scheelite-1 in retrograde stage and scheelite-2 from sulfide-stage exhibit similar fluid compositions, and the lower K content in the second stage is thought to be caused by sericitization in the retrograde stage. A variable redox condition was also recorded for different stages of economic scheelite, indicating that fluid oxygen fugacity is likely negligible for scheelite precipitation.

(4) Magmatic fluid identical in chemistry revealed by fluid inclusions data is responsible for the formation of both W mineralization styles at Yaogangxian. Combined with previous geological and geochronological studies, a metallogenic model of the coupled wolframite-quartz vein and scheelite-skarn mineralization has been established. We propose that the Ca responsible for the precipitation of scheelite in the Yuxin section is primarily contributed by carbonate, whereas the Fe necessary for wolframite deposition may in part come from alteration of the host rock, or come directly from the magma. Further qualification of the composition of the fluid prior to wolframite precipitation is the key to addressing this issue.

Declaration of Competing Interest

The authors declare that they have no known competing financial interests or personal relationships that could have appeared to influence the work reported in this paper.

Data availability

Data will be made available on request.

Acknowledgements

This work is financially supported by National Natural Science Foundation of China (Grant Nos. 41830426, 92062220, 42202064), the Fundamental Research Funds for the Central Universities (Grant No. 2023300131, 2021300199, 2022300300) and the Foundation Research Projects of Jiangsu Province (Grant No. BK20201258, BK20200325). We are grateful to Yan Gao, Jianming Cui and Liang Han at Nanjing University for helping with field sampling and fluid inclusion measurement.

Appendix A. Supplementary data

Supplementary data to this article can be found online at https://doi.org/10.1016/j.oregeorev.2023.105544.

References

Brown, P.E., Essene, E.J., 1985. Activity variations attending tungsten skarn formation, Pine Creek, California. Contrib. Mineral. Petrol. 89 (4), 358–369.
Carocci, E., Marignac, C., Cathelineau, M., Truche, L., Poujol, M., Boiron, M.C., Pinto, F., 2020. Incipient wolframite deposition at Panasqueira (Portugal): W-rich rutile and tourmaline compositions as proxies for the early fluid composition. Econ. Geol. 116, 123–146.
Chang, Z.S., Shu, Q.H., Meinert, L.D., 2019. Skarn deposits of China. Soc. Econ. Geol. Special Publ. 22, 189–234.
Chen, L.L., Ni, P., Dai, B.Z., Li, W.S., Chi, Z., Pan, J.Y., 2019. The genetic association between quartz vein- and greisen-type mineralization at the Maoping W-Sn deposit, Southern Jiangxi, China: insights from Zircon and Cassiterite U-Pb Ages and Cassiterite Trace Element Composition. Minerals 9, 1–24.
Chen, J., Wang, R., Zhu, J., Lu, J., Ma, D., 2013. Multiple-aged granitoids and related tungsten-tin mineralization in the Nanling Range, South China. Sci. China Ear. Sci. 56 (12), 2045–2055.
Choi, W., Park, C., Song, Y., 2020. Multistage W-mineralization and magmatic-hydrothermal fluid evolution: Microtextural and geochemical footprints in scheelite from the Weondong W-skarn deposit, South Korea. Ore Geol. Rev. 116, 103219.
Dick, L.A., Hodgson, C.J., 1982. The MacTung W-Cu(Zn) contact metasomatic and related deposits of the northeastern Canadian Cordillera. Econ. Geol. 77, 845–867.
Fall, A., Bodnar, R.J., 2018. How precisely can the temperature of a fluid event be constrained using fluid inclusions? Econ. Geol. 113, 1817–1843.
Fonteilles, M., Soler, P., Demange, M., Derre, C., Krier-Schellen, A.D., Verkaeren, J., Guy, B., Zahm, A., 1989. The scheelite skarn deposit of Salau (Ariege, French Pyrenees). Econ. Geol. 84, 1172–1209.
Goldstein, R.H., Reynolds, T.J., 1994. Systematics of fluid inclusions in diagenetic mineral. Tulsa, Okla. SEPM 69–85.
Goldstein, R.H., 2003. Petrographic analysis of fluid inclusions: Mineralogical Association Canada Short Course 32, 9–53.
Guillong, M., Meier, D.L., Allan, M.M., Heinrich, C.A., Yardley, B.W.D., 2008. SILLS: a Matlab-based program for the data reduction of laser ablation ICP-MS data of homogeneous materials and inclusions. Mineral Assoc. Canada 40, 328–333.
Han, L., Pan, J.Y., Ni, P., Chen, H., 2023. Cassiterite deposition induced by cooling of a single-phase magmatic fluid: Evidence from SEM-CL and fluid inclusion LA-ICP-MS analysis. Geochim. Cosmochim. Acta 342, 108–127.
Hayes, S.M., McCullough, E.A., 2018. Critical minerals: A review of elemental trends in comprehensive criticality studies. Resour. Policy 59, 192–199.
He, X., Zhang, D.a., Di, Y., Wu, G., Hu, B., Huo, H., Li, N., Li, F., 2022. Evolution of the magmatic–hydrothermal system and formation of the giant Zhuxi W-Cu deposit in South China. Geosci. Front. 13 (1), 101278.
Heinrich, C.A., Pettke, T., Halter, W.E., Aigner-Torres, M., Audétat, A., Günther, D., Hattendorf, B., Bleiner, D., Guillong, M., Horn, I., 2003. Quantitative multi-element analysis of minerals, fluid and melt inclusions by laser-ablation inductively-coupled-plasma mass-spectrometry. Geochim. Cosmochim. Acta 67 (18), 3473–3497.
Hsu, L., 1977. Effects of oxygen and sulfur fugacities on the scheelite-tungstenite and powellite-molybdenite stability relations. Econ. Geol. 72, 664–670.
Hu, R.-Z., Zhou, M.-F., 2012. Multiple Mesozoic mineralization events in South China—an introduction to the thematic issue. Miner. Depos. 47 (6), 579–588.
Hulsbosch, N., Boiron, M.C., Dewaele, S., Muchez, P., 2016. Fluid fractionation of tungsten during granite–pegmatite differentiation and the metal source of peribatholitic W quartz veins: evidence from the Karagwe-Ankole Belt (Rwanda). Geochim. Cosmochim. Acta 175, 299–318.
Ishihara, S., Wang, P., Kajiwara, Y., Watanabe, Y., 2003. Origin of sulfur in some magmatic-hydrothermal ore deposits of South China. Bull. Geol. Surv. Jpn. 54 (3-4), 161–169.
Jiang, H., Jiang, S.Y., Li, W.Q., Zhao, K.D., Peng, N.J., 2018. Highly fractionated Jurassic I-type granites and related tungsten mineralization in the Shirenzhang deposit, northern Guangdong, South China: evidence from cassiterite and zircon U-Pb ages, geochemistry and Sr-Nd-Pb-Hf isotopes. Lithos 312–313, 186–203.
Jiang, H., Liu, B., Kong, H., Wu, Q.-H., Chen, S., Li, H., Wu, J.-H., 2022. In situ geochemistry and Sr–O isotopic composition of wolframite and scheelite from the Yaogangxian quartz vein-type W(–Sn) deposit, South China. Ore Geol. Rev. 149, 105066.
Kelly, W.C., Rye, R.O., 1979. Geologic, fluid inclusion, and stable isotope studies of the tin-tungsten deposits of Panasqueira, Portugal. Econ. Geol. 74, 1721–1822.
Klemm, L.M., Pettke, T., Heinrich, C.A., 2008. Fluid and source magma evolution of the Questa porphyry Mo deposit, New Mexico, USA. Miner. Deposita 43 (5), 533–552.
Korges, M., Weis, P., Lüders, V., Laurent, O., 2017. Depressurization and boiling of a single magmatic fluid as a mechanism for tin-tungsten deposit formation. Geology 46, 75–78.
Kwak, T.A.P., Tan, T.H., 1981. The geochemistry of zoning in skarn minerals at the King Island (Dolphin) Mine. Econ. Geol. 76, 468–497.
Launay, G., Sizaret, S., Lach, P., Melleton, J., Gloaguen, É., Poujol, M., 2021. Genetic relationship between greisenization and Sn-W mineralizations in vein and greisen deposits: Insights from the Panasqueira deposit (Portugal). Bull. Soc. Géol. France 192.
Layne, G.D., Spooner, E.T.C., 1991. The JC tin skarn deposit, southern Yukon Territory; I, Geology, paragenesis, and fluid inclusion microthermometry. Econ. Geol. 86, 29–47.
Lecumberri-Sanchez, P., Vieira, R., Heinrich, C.A., Pinto, F., Wälle, M., 2017. Fluid-rock interaction is decisive for the formation of tungsten deposits. Geology 45 (7), 579–582.
Legros, H., Richard, A., Tarantola, A., Kouzmanov, K., Mercadier, J., Vennemann, T., Marignac, C., Cuney, M., Wang, R.C., Charles, N., Bailly, L., Lespinasse, M.Y., 2019. Multiple fluids involved in granite-related W-Sn deposits from the world-class Jiangxi province (China). Chem. Geol. 508, 92–115.
Li, S.T., Wang JB, Zhu XY, Wang YL, Han Y, Guo LL (2011) Chronological characteristics of the Yaogangxian composite pluton in Hunan Province. Geol. Explor. 47:143–215 (in Chinese with English abstract).
Li, W.S., Ni, P., Pan, J.Y., Wang, G.G., Chen, L.L., Yang, Y.L., Ding, J.Y., 2018. Fluid inclusion characteristics as an indicator for tungsten mineralization in the Mesozoic Yaogangxian tungsten deposit, central Nanling district, South China. J. Geochem. Explor. 192, 1–17.
Li, W.-S., Ni, P., Wang, G.-G., Yang, Y.-L., Pan, J.-Y., Wang, X.-L., Chen, L.-L., Fan, M.-S., 2020. A possible linkage between highly fractionated granitoids and associated W-mineralization in the Mesozoic Yaogangxian granitic intrusion, Nanling region, South China. J. Asian Earth Sci. 193, 104314.
Li, W.-S., Ni, P., Pan, J.-Y., Fan, M.-S., Chen, L.-L., Zhang, D.i., Wu, X.-W., Gao, Y., 2021. Constraints on the timing and genetic link of scheelite- and wolframite-bearing quartz veins in the Chuankou W ore field, South China. Ore Geol. Rev. 133, 104122.
Li, W.-S., Ni, P., Pan, J.-Y., De Vivo, B., Albanese, S., Fan, M.-S., Gao, Y., Zhang, D.-X., Chi, Z., 2022a. Co-genetic formation of scheelite- and wolframite-bearing quartz veins in the Chuankou W deposit, South China: Evidence from individual fluid inclusion and wall-rock alteration analysis. Ore Geol. Rev. 142, 104723.
Li, W.S., Ni, P., Zeng, Z.L., Peng, Z.Q., Pan, J.Y., Fan, M.S., Zhang, K.H., Liu, Z., Zhang, D., Cui, J.M., Zhao, L.Q., 2022b. In situ zircon and cassiterite U-Pb ages constraints on concealed granite and W mineralization in the Kuimeishan deposit, Nanling Region, South China. J. Geochem. Explor. 240, 107043.
Li, Y., Pan, J.Y., Wu, L.G., He, S., Bachmann, O., Li, X.H., 2023. Transient tin mineralization from cooling of magmatic fluids in a long-lived system. Geology.
Liu, J.-X., Wang, S., Wang, X.-L., Du, D.-H., Xing, G.-F., Fu, J.-M., Chen, X., Sun, Z.-M., 2020. Refining the spatio-temporal distributions of Mesozoic granitoids and volcanic rocks in SE China. J. Asian Earth Sci. 201, 104503.
Lu, H.-Z., Liu, Y., Wang, C., Xu, Y., Li, H., 2003. Mineralization and fluid inclusion study of the Shizhuyuan W-Sn-Bi-Mo-F Skarn Deposit, Hunan Province. China. Econ. Geol. 98 (5), 955–974.
Mao, J. W., Ouyang, H. G., Song, S. W., Santosh, M., Yuan, S. D., Zhou, Z. H., Zheng, W., Liu, H., Liu, P., Cheng, Y. B., Chen, M. H., 2019. Geology and Metallogeny of Tungsten and Tin Deposits in China. SEG Special Publications 22, 411–482.
Mao, J.W., Xie, G.Q., Guo, C.L., Chen, Y.C., 2007. Large–scale tungsten–tin mineralization in the Nanling region, South China: metallogenic ages and corresponding geodynamic processes. Acta Petrol. Sin. 23, 2329–2338 in Chinese with English abstract.
Meinert, L.D., Dipple, G.M., Nicolescu, S., 2005. World Skarn Deposits, in: Hedenquist, J. W., Thompson, J.F.H., Goldfarb, R.J., Richards, J.P. (Eds.), One Hundredth Anniversary Volume. Society of Economic Geologists 299–336.
Miranda, A.C.R., Beaudoin, G., Rottier, B., 2022. Scheelite chemistry from skarn systems: implications for ore-forming processes and mineral exploration. Miner. Deposita 57 (8), 1469–1497.
Nast, H.J., Williams-Jones, A.E., 1991. The role of water-rock interaction and fluid evolution in forming the porphyry-related Sisson Brook W-Cu-Mo deposit, New Brunswick. Econ. Geol. 86, 302–317.
Newberry, R.J., 1983. The formation of subcalcic garnet in scheelite-bearing skarns. Can. Mineral. 21, 529–544.
Ni, P., Wang, X.D., Wang, G.G., Huang, J.B., Pan, J.Y., Wang, T.G., 2015. An infrared microthermometric study of fluid inclusions in coexisting quartz and wolframite

from Late Mesozoic tungsten deposits in the Gannan metallogenic belt, South China. Ore Geol. Rev. 65, 1062–1077.
Ni, P., Li, W.S., Pan, J.Y., 2020. Ore-forming fluid and metallogenic mechanism of wolframite-quartz vein-type tungsten deposits in South China. Acta Geol. Sin-Engl. Ed. 94, 1774–1796.
Ni, P., Wang, G.G., Li, W.S., Chi, Z., Li, S.N., Gao, Y., 2021. A review of the Yanshanian ore-related felsic magmatism and tectonic settings in the Nanling W-Sn and Wuyi Au-Cu metallogenic belts, Cathaysia Block, South China. Ore Geol. Rev. 133, 18.
Ni, P., Pan, J.-Y., Han, L., Cui, J.-M., Gao, Y., Fan, M.-S., Li, W.-S., Chi, Z., Zhang, K.-H., Cheng, Z.-L., Liu, Y.-P., 2023. The tungsten and tin deposits in South China: temporal and spatial distribution, metallogenic models and prospecting directions. Ore Geol. Rev. 157, 105453.
Oyunjargal, L., Matsukura, K., Hayashi, K.-I., 2019. Oxygen isotopic study on the Date-Nagai Skarn-Type Tungsten Deposit, Northeastern Japan Resour. Geol. 69 (4), 448–459.
Pan, J.Y., Ni, P., Wang, R.C., 2019. Comparison of fluid processes in coexisting wolframite and quartz from a giant vein-type tungsten deposit, South China: Insights from detailed petrography and LA-ICP-MS analysis of fluid inclusions. Am. Mineral. 104, 1092–1116.
Peng, J., Zhou, M.-F., Hu, R., Shen, N., Yuan, S., Bi, X., Du, A., Qu, W., 2006. Precise molybdenite Re-Os and mica Ar-Ar dating of the Mesozoic Yaogangxian tungsten deposit, central Nanling district, South China. Miner. Deposita 41 (7), 661–669.
Pettke, T., Oberli, F., Audétat, A., Guillong, M., Simon, A.C., Hanley, J.J., Klemm, L.M., 2012. Recent developments in element concentration and isotope ratio analysis of individual fluid inclusions by laser ablation single and multiple collector ICP-MS. Ore Geol. Rev. 44, 10–38.
Poblete, J.A., Dirks, P.H.G.M., Chang, Z.S., Huizenga, J.M., Griessmann, M., Hall, C., 2021. The watershed tungsten deposit, northeast Queensland, australia: permian metamorphic tungsten mineralization overprinting carboniferous magmatic tungsten. Econ. Geol. 116, 427–451.
Poulin, R.S., McDonald, A.M., Kontak, D.J., McClenaghan, M.B., 2016. On the relationship between cathodoluminescence and the chemical composition of scheelite from geologically diverse ore-deposit environments. Can. Mineral. 54 (5), 1147–1173.
Raimbault, L., Baumer, A., Dubru, M., Benkerrou, C., Croze, V., Zahm, A., 1993. REE fractionation between scheelite and apatite in hydrothermal conditions. Am. Miner. 78, 1275–1285.
Sanchez, S.M.T., Benito, M.C.M., Perez, M.L.C., 2009. Mineralogical and physiochemical evolution of the Los Santos Scheelite Skarn, Salamanca, NW Spain. Econ. Geol. 104 (7), 961–995.
Seo, J.H., Guillong, M., Aerts, M., Zajacz, Z., Heinrich, C.A., 2011. Microanalysis of S, Cl, and Br in fluid inclusions by LA-ICP-MS. Chem. Geol. 284, 35–44.
Shu, L., Yao, J., Wang, B., Faure, M., Charvet, J., Chen, Y., 2021. Neoproterozoic plate tectonic process and Phanerozoic geodynamic evolution of the South China Block. Earth-Sci. Rev. 216, 103596.
Singoyi, B., Zaw, K., 2001. A petrological and fluid inclusion study of magnetite–scheelite skarn mineralization at Kara, Northwestern Tasmania: implications for ore genesis. Chem Geol 173 (1-3), 239–253.
Soloviev, S.G., Kryazhev, S.G., 2017. Geology, mineralization, and fluid inclusion characteristics of the Skrytoe reduced-type W skarn and stockwork deposit, Sikhote-Alin, Russia. Miner. Deposita 52 (6), 903–928.
Soloviev, S.G., Kryazhev, S.G., 2019. Geology, mineralization, and fluid inclusion characteristics of the Koitash redox-intermediate W-Mo skarn and W–Au stockwork deposit, western Uzbekistan, Tien Shan. Miner. Deposita 54, 1179–1206.
Song, G., Qin, K., Li, G., Evans, N.J., Chen, L., 2014. Scheelite elemental and isotopic signatures: implications for the genesis of skarn-type W-Mo deposits in the Chizhou Area, Anhui Province, Eastern China. Am. Miner. 99 (2-3), 303–317.
Timón, S.M., Moro, M.C., Cembranos, M.L., Fernández, A., Crespo, J.L., 2007. Contact metamorphism in the Los Santos W skarn (NW Spain). Mineral Petrol. 90 (1-2), 109–140.
Tornos, F., Galindo, C., Spiro, B.F., 2001. Isotope geochemistry of Los Santos (Spanish Central System) calcic scheelite skarn: constraints on the source of the fluids and tungsten. Piestrzynski (Eds) Mineral Deposits at the Beginning of the 21st Century Swets & Zeitlinger Publishers Lisse 921–924.
Tornos, F., Galindo, C., Crespo, J.L., Spiro, B.F., 2008. Geochemistry and origin of calcic tungsten-bearing skarns, Los Santos, Central Iberian Zone, Spain. Can. Mineral 46 (1), 87–109.
Wang, X., Ren, M.H., 2018. Constraints of hydrothermal and magmatic zircon on the origin of the Yaogangxian tungsten deposit, Southern China. Ore Geol. Rev. 101, 453–467.
Wang, X.S., Timofeev, A., Williams-Jones, A.E., Shang, L.B., Bi, X.W., 2019. An experimental study of the solubility and speciation of tungsten in NaCl-bearing aqueous solutions at 250, 300, and 350 °C. Geochim. Cosmochim. Acta 265, 313–329.
Wang, Y.L., Zhu, X.Y., Cheng, X.Y., Li, S.T., 2014. Comparative study of the ore-forming fluids in the two types of tungsten deposits in Yaogangxian, Hunan. Mineral Explor. 5, 728–737. In Chinese with English abstract.
Wood, S.A., Samson, I.M., 2000. The hydrothermal geochemistry of tungsten in granitoid environments: I. Relative solubilities of ferberite and scheelite as a function of T, P, pH, and mNaCl. Econ. Geol. 95 (1), 143–182.
Xiao, M., Qiu, H.-N., Cai, Y., Jiang, Y.-D., Zhang, W.-F., Fang, Y., 2021. Progressively released gases from fluid inclusions reveal new insights on W-Sn mineralization of the Yaogangxian tungsten deposit, South China. Ore Geol. Rev. 138, 104353.
Xu, K.C., 1957. Discovery of pyrometasomatic scheelite deposits near a wolframite-producing district in Southern China, and a discussion about the origin of these two classes of deposits. Acta Geol. Sinia 37, 117–151 in Chinese with English abstract.
Yang, Y.L., Ni, P., Pan, J.Y., Wang, G.G., Xu, Y.F., 2017. Constraints on the mineralization processes of the Makeng iron deposit, eastern China: Fluid inclusion, H-O isotope and magnetite trace element analysis. Ore Geol. Rev. 88, 791–808.
Yu, Z.F., Zhao, Z., Wang, Y.L., Zhu, X.Y., Yin, Z., Li, H.W., 2021. Characteristics and evolutions of ore-forming fluids in the Yaogangxian skarn-type scheelite deposit, Hunan Procince. Acta Petrol. Sin. 38, 513–528 in Chinese with English abstract.
Yuan, L.L., Chi, G.X., Wang, M.Q., Li, Z.H., Xu, D.R., Deng, T., Geng, J.Z., Hu, M.Y., Zhang, L., 2019a. Characteristics of REEs and trace elements in scheelite from the Zhuxi W deposit, South China: implications for the ore-forming conditions and processes. Ore Geol Rev. 109, 585–597.
Yuan, S.D., Williams-Jones, A.E., Romer, R.L., Zhao, P.L., Mao, J.W., 2019b. Protolith-related thermal controls on the decoupling of Sn and W in Sn-W metallogenic provinces: insights form the Nanling region, China. Econ. Geol. 114, 1005–1012.
Zaw, K., Singoyi, B., 2000. Formation of magnetite-scheelite skarn mineralization at Kara, Northwestern Tasmania: evidence from mineral chemistry and stable isotopes. Econ. Geol. 95, 1215–1230.
Zhao, W.W., Zhou, M.F., Li, Y.H.M., Zhao, Z., Gao, J.F., 2017. Genetic types, mineralization styles, and geodynamic settings of Mesozoic tungsten deposits in South China. J. Asian Earth Sci. 137, 109–140.
Zhou, X., Sun, T., Shen, W., Shu, L., Niu, Y., 2006. Petrogenesis of Mesozoic granitoids and volcanic rocks in South China: A response to tectonic evolution. Episodes 29 (1), 26–33.
Zhu, X.Y., Wang, Y.L., Cheng, X.Y., Tian, Y., Fu, Q.B., Li, S.T., 2015a. Metallogenic system of Yaogangxian quartz vein type tungsten ore deposit in Hunan. Mineral Deposits 34, 874–894 (in Chinese with English abstract).
Zhu, X.Y., Wang, J.B., Wang, Y.L., Chen, X.Y., Fu, Q.B., Tian, Y., 2015a. The differences of the ore-forming fluid between the vein-type and skarn type tungsten deposits. Acta Petrol Sin. 31, 941–953 in Chinese with English abstract.